

PAPER

PDeepPP: A Deep learning framework with Pretrained Protein language for peptide classification

Jixiu Zhai^{2,†}, Tianchi Lu^{1,†,*}, Haitian Zhong³, Ziyang Xu⁴, Yuhuan Liu⁵, Xueying Wang^{1,6}, Dan Huang⁷

¹Department of Computer Science, City University of Hong Kong, Kowloon, Hong Kong, ²School of Mathematics and Statistics, Lanzhou University, 222 South Tianshui Road, Lanzhou 730000, China, ³New Laboratory of Pattern Recognition (NLPR), State Key Laboratory of Multimodal Artificial Intelligence Systems (MAIS), Institute of Automation, Chinese Academy of Sciences (CASIA), ⁴Department of Mathematics, The Chinese University of Hong Kong, Hong Kong, China, ⁵Cuiying Honors College, Lanzhou University, 222 South Tianshui Road, Lanzhou 730000, China, ⁶Department of Computer Science, City University of Hong Kong (Dongguan), Dongguan 523000, China and ⁷Department of Mathematics, Harbin Engineering University, No. 145 Nantong Street, Harbin 150001, China

*Corresponding author. tianchilu4-c@my.cityu.edu.hk

FOR PUBLISHER ONLY Received on Date Month Year; revised on Date Month Year; accepted on Date Month Year

Abstract

Protein post-translational modifications (PTMs) and bioactive peptides (BPs) play critical roles in various biological processes and have significant therapeutic potential. However, identifying PTM sites and bioactive peptides through experimental methods is often labor-intensive, costly, and time-consuming. As a result, computational tools, particularly those based on deep learning, have become effective solutions for predicting PTM sites and peptide bioactivity. Despite progress in this field, existing methods still struggle with the complexity of protein sequences and the challenge of requiring high-quality predictions across diverse datasets. To address these issues, we propose a deep learning framework that integrates pretrained protein language models with a neural network combining transformer and CNN for peptide classification. By leveraging the ability of pretrained models to capture complex relationships within protein sequences, combined with the predictive power of parallel networks, our approach improves feature extraction while enhancing prediction accuracy. This framework was applied to multiple tasks involving PTM site and bioactive peptide prediction, utilizing large-scale datasets to enhance the model's robustness. In the comparison across 33 tasks, the model achieved state-of-the-art (SOTA) performance in 25 of them, surpassing existing methods and demonstrating its versatility across different datasets. Our results suggest that this approach provides a scalable and effective solution for large-scale peptide discovery and PTM analysis, paving the way for more efficient peptide classification and functional annotation.

Key words: pretrained language model, deep learning, transformer, protein sequence classification

Introduction

In recent years, biological feature prediction technology has gradually matured(1; 2; 3), Protein post-translational modifications (PTMs)(4; 5; 6) and bioactive peptides (BPs)(7; 8) play crucial roles in various biological processes, profoundly impacting cellular regulation, protein functionality, and therapeutic advancements. These modifications and peptides have gained tremendous attention from both researchers and consumers, driven by increasing demand for natural therapeutics, concerns over synthetic products, and sustainability considerations. The global BPs market is expected to double from 48.6 billion USD in 2020 to 95.7 billion USD by 2028, with applications spanning drugs, nutraceuticals and cosmeceuticals(9; 10). PTMs, such as phosphorylation(11), glycosylation(12), or acetylation(13), are chemical modifications that occur post-synthesis and influence cellular signaling and protein dysfunction, which are

closely linked to a range of diseases(14). Similarly, bioactive peptides(15), composed of short amino acid sequences, exhibit various biological activities such as antimicrobial, anticancer, and antioxidant effects, making them a focal point in pharmaceutical research. These peptides can be produced from sustainable food protein sources through enzymatic hydrolysis or fermentation, offering a promising avenue for developing natural therapeutic agents(16; 17).

However, traditional experimental methods for identifying PTM sites(18; 19; 20) and bioactive peptides(21; 22) are resource-intensive, time-consuming, and costly. In recent years, computational tools, including deep learning models such as MusiteDeep(23; 24; 25; 26), UniDL4BioPep(27) or prediction optimization for a single modification type(28; 29; 30) have made significant progress, showing promise in improving predictive performance(31; 32) The development of deep learning has further strengthened its role in

biopharmaceuticals, with increasingly mature technologies that support drug discovery, biomarker identification, and precision medicine(33; 34; 35). Despite these advancements, existing models still face challenges, including poor generalization across diverse datasets, limited support for large-scale tasks, difficulties in adapting to imbalanced datasets, and specificity for certain PTM types or peptide functionalities, which hinder their broader application.

To overcome these limitations, we introduce PDeepPP, a novel deep learning framework that integrates pretrained protein language models (e.g., ESM-2(36)) with weighted parallel neural networks based on transformer(37) and convolutional neural network (CNN)(38) architectures, combined with a Transductive Information Maximization (TIM) loss function(39; 40) tailored for imbalanced datasets, providing a highly efficient and scalable solution for peptide classification and PTM prediction. By leveraging ESM-2 to extract rich contextual features from large-scale protein sequence data without the need for extensive feature engineering, PDeepPP captures both local and global sequence complexities. The integration of transformer-based global feature chains with CNN-based local feature chains further improves predictive accuracy while maintaining computational efficiency. Through extensive experiments, PDeepPP has demonstrated superior performance across multiple benchmark datasets, improving accuracy and robustness while reducing false positives and negatives. This framework showcases its potential as a transformative tool in peptide discovery and PTM annotation.

Materials and methods

Benchmark datasets

All benchmark datasets are sourced from existing review papers and datasets used for single-task predictions. We conducted a fair evaluation of metrics on the collected datasets. In total, we collected 37 datasets from two review articles and four single-task papers, including twenty BPs datasets for seventeen different bioactivities and 17 PTMs datasets for different modifications. Specifically contains angiotensin converting enzyme (ACE) inhibitory activity (anti-hypertension)(41), dipeptidyl peptidase (DPPIV) inhibitory activity (anti-diabetes)(42), bitter (43), umami(44), antimicrobial activity (45), antimalarial activity(46), quorum-sensing (QS) activity(47), anticancer activity(48; 49), anti-methicillin-resistant *S. aureus* (MRSA) strains activity (50), tumor T cell antigens (TTCA)(51), blood-brain barrier(52), antiparasitic activity (53), neuropeptide(54; 55), antibacterial activity (56), antifungal activity (56), antiviral activity(56), toxicity(57) and antioxidant(58) activity ;The following data are all derived from the UniProtKB/Swiss-Prot database(59): Phosphoserine/threonine, Phosphotyrosine, N-linked glycosylation, O-lined glycosylation, N6-acetyllysine, Methyllysine, S-palmitoylation-cysteine, Pyrrolidone-carboxylic-acid, Ubiquitination, SUMOylation, Hydroxylysine, Hydroxyproline, methyl-Glutamines(60), methylation-arginine(61), Ubiquitin_K(62) and histone lysine crotonylation(63). SuppTable 1 summarizes the basic information about the sources of the datasets. More information and the complete data can be found on [github].

Structure overview

Recent hybrid architectures (64; 65) demonstrate that combining ESM with task-specific embeddings improves PTM generalization. PDeepPP uses a parallel neural network with CNNs and

Transformers for module combination. The TransLinear layer uses the combination of encoder and fully connected layer, and the PosCNN layer uses the combination of position encoding and CNN. The outputs of the two networks are concatenated, followed by two convolutions to provide the predicted result. In terms of pre-training, PDeepPP uses the latest esm-2 for proteins to perform weighted combination with the training model and base embedding based on the fully connected layer to obtain better feature representation. The entire process used by PDeepPP is referenced in Fig. 1.

Data processing

For the benchmark data set, the original data set that was not divided was taken out according to the ratio of 20%. New results show that long sequences of proteins can enhance learning of molecular interactions,(66)so the sequence was cut at the same time, and every 33 consecutive amino acids were cut into a sequence. Sequences of insufficient length are padded with X, and partial overlap of sequences is allowed. For PTM sites, the positive site should be placed in the middle of the sequence. If there is a peptide chain of less than 33 amino acids, its ends are padded to the target length before training. The validation set is randomly selected at training time according to 10% of the training set.

Embedding strategy

The model used in this work is ESM-2 with 650 million parameters, a large-scale pre-trained model designed to capture the complex relationships within protein sequences through a Transformer architecture. ESM-2 is pre-trained using a Masked Language Modeling (MLM) objective on a large protein sequence dataset, enabling it to learn both local and global sequence dependencies. The model generates token-wise embeddings that provide rich contextual representations of proteins, which are particularly effective for tasks such as protein structure prediction and functional annotation.

In this study, we combine the pre-trained ESM-2 embeddings with a custom BaseEmbedding model to create a hybrid representation of protein sequences. BaseEmbedding pre-training is an embedding layer with a separate teleprompter that generates additional sequence representations, which are linearly transformed to match the ESM-2 output dimension (1280). This combination aims to leverage the pre-trained knowledge from ESM-2 while allowing the model to learn task-specific embeddings through the BaseEmbedding.

Moreover, residual connections are introduced between these two representations to facilitate feature refinement and ensure efficient gradient propagation, a design choice shown to improve training stability and overall performance in deep neural networks(67; 68).

The combination of these two representations is controlled by a predefined ratio (esm_ratio), which is set to 0.9 in this case. This means that 90% of the final representation comes from the ESM-2 embeddings, while 10% comes from the BaseEmbedding model. The final combined sequence representation is computed using the following weighted sum:

$$R_{\text{combined}} = \alpha \cdot R_{\text{ESM-2}} + (1 - \alpha) \cdot R_{\text{Base}}$$

where:

R_{combined} represents The combined sequence feature representation; α (set to 0.9) is the 'esm_ratio', which defines the contribution of the ESM-2 embeddings; $R_{\text{ESM-2}}$ is the embedding generated

by the ESM-2 model; R_{Base} is the embedding generated by the BaseEmbedding model.

This hybrid representation allows the model to retain the rich, pre-trained features from ESM-2 while incorporating learnable, task-specific features from BaseEmbedding. The process of generating the combined sequence embeddings involves several steps:

ESM-2 Embeddings

Protein sequences are passed through the pre-trained ESM-2 model, which generates token-wise embeddings from its final layer. ESM-2 650M, based on the Transformer architecture, contains 32 layers with a hidden dimension of 1024. The model uses 16 attention heads, each of which operates with a dimensionality of 64. The feedforward network has a dimension of 2048. The model's input layer embeds protein sequences into 1024-dimensional vectors, while the output consists of embeddings for each amino acid position in the sequence. These embeddings capture long-range dependencies within protein sequences, providing crucial information for tasks such as protein structure and function prediction. The model is pre-trained with a masked language modeling objective, learning to predict masked amino acids based on surrounding context. The resulting embeddings effectively encode the structural and functional features of the protein sequences, enabling downstream applications such as protein classification, function annotation, and structure prediction.⁽⁶⁹⁾

BaseEmbedding Model

The BaseEmbedding model consists of a learnable embedding layer that maps each amino acid in the sequence to a 128-dimensional high-dimensional vector. This vector is subsequently transformed through a linear layer to produce a 1280-dimensional representation, aligning it with the dimensionality of the ESM-2 embeddings.

Sequence Padding

Protein sequences vary in length, so they are padded to ensure uniformity across batches. Each sequence is padded to match the maximum sequence length in the dataset, allowing for efficient batch processing.

Weighted Combination

The embeddings generated by the ESM-2 model and the BaseEmbedding model are combined using the predefined ratio ($\text{esm_ratio} = 0.9$). The combined sequence representation is computed as shown in the formula above, where the ESM-2 embeddings contribute 90% of the final representation and the BaseEmbedding model contributes 10%.

Saving Representations

The combined representations for both the training and test datasets are saved as .numpy files for use in downstream tasks. The corresponding labels are also saved, ensuring that the representations can be easily loaded and utilized for further model training or evaluation. This approach, which combines a powerful pre-trained model with a learnable embedding layer, provides a flexible and effective method for representing protein sequences. It allows the model to adapt to specific tasks while benefiting from the pre-trained knowledge encoded in the ESM-2 model.

TransConv1d Network

The TransConv1d layer combines self-attention mechanisms, a Transformer encoder, and fully connected networks to extract global and local features from input data, making it suitable for processing sequential data or high-dimensional features. Its architecture consists of multiple modules, each with specific hyperparameters to ensure the model's expressive power and training stability.

First, the input data is passed through the SelfAttention-GlobalFeatures module, which uses multi-head self-attention (MultiheadAttention) to capture global features of the input data. Specifically, the [embed_dim] is set to the input feature dimension, and [num_heads] is set to 8 to parallelize the processing of different feature patterns. The output of the self-attention is added to the original input via a residual connection and then stabilized with layer normalization (LayerNorm). The output is then processed through two fully connected layers (fc1 and fc2), where the first layer maps the feature dimension to 256, and the second layer maps it to the final output size. Dropout is applied after the first fully connected layer to prevent overfitting.

Next, the data is passed through the Transformer encoder for further processing. The encoder consists of 4 Transformer encoder layers, each with a model dimension (d_model) of output_size, and uses 8 attention heads (nhead=8) to handle the input data. The feedforward network has a dimension of 512, and 0.3 dropout is applied at each layer to prevent overfitting. The Transformer encoder further learns the global dependencies in the input data and extracts deeper-level features.

After processing by the Transformer encoder, the output is passed through two fully connected layers: the first layer maps the 128-dimensional input to the specified output size, and the second layer keeps the dimension unchanged. A residual connection adds the output of the second layer to the first layer's output, ensuring the preservation of early feature information. Finally, layer normalization (LayerNorm) is applied to the result to stabilize the output and improve the training efficiency.

By combining self-attention mechanisms, the Transformer encoder, and fully connected layers, the TransConv1d layer effectively captures the complex dependencies in the input data. The residual connections and layer normalization help maintain data stability and preserve information, thus improving the model's expressive power and training stability.

PosCNN Network

The PosCNN layer integrates convolutional neural network (CNN) operations with optional positional encoding, designed to extract local features from input data while preserving sequence information, making it suitable for processing sequential data or high-dimensional features. The architecture focuses on capturing local patterns through convolution operations, followed by a fully connected layer for feature mapping.

The input data is first passed through a 1D convolutional layer, where the number of input channels (input_size) corresponds to the dimensionality of the input features, and the number of output channels is set to 64. The convolution operation uses a kernel size of 3 and padding of 1 to preserve the sequence length. After the convolution, a ReLU activation function is applied to introduce non-linearity, enhancing the model's expressive capability.

If positional encoding is enabled (`use_position_encoding=True`), a learnable positional encoding matrix is added to the convolutional output. This matrix has a shape of $64 \times$ sequence length and is applied through broadcasting. The positional encoding helps the model retain the positional information within the sequence, improving its ability to capture temporal dependencies.

Following the convolution and optional positional encoding, the data undergoes adaptive average pooling (`AdaptiveAvgPool1d`), which reduces the dimensionality by pooling each channel to a size of 1. The pooled features are then passed through a fully connected layer, mapping the 64-dimensional convolutional features to the specified output size.

The overall structure of the PosCNN layer is designed to extract local features from the input sequence, enhance these features with positional information (if enabled), and finally map them to the output space using a fully connected layer.

PredictModule

The forward process of the PredictModule first processes the input data x through the `TransConv1d` and `PosCNN` layers to obtain two feature representations. The outputs are then adjusted in dimension and concatenated along the feature dimension, forming a unified representation that combines both global and local features. The concatenated features are then permuted to match the input format required by the subsequent convolutional layers. The combined output from `TransConv1d` and `PosCNN` is passed through a convolutional layer with 32 output channels, followed by adaptive max pooling to reduce the sequence length to 1, with dropout applied for regularization. Next, the processed features are passed through another convolutional layer with 64 output channels, followed by max pooling and dropout. Finally, the features are flattened and input into a fully connected layer to generate the final prediction output. This sequence of operations helps refine the features, prevent overfitting, and produce robust prediction results.

Loss function

In our training process, we employed the **Transductive Information Maximization (TIM) loss function**(39). The TIM loss integrates the traditional Cross-Entropy Loss (CE) with an empirically weighted Mutual Information term. The goal of the TIM loss is to minimize the difference between the predicted and true label distributions while maximizing the mutual information between the input data and the labels. Research has shown that mutual information can effectively capture complex, non-linear dependencies in high-dimensional data, thereby enhancing feature representations and improving overall model robustness(70; 71).

The mutual information component is divided into two main terms: the marginal entropy of the labels and the conditional entropy of the labels given the input data. The empirical mutual information can be expressed as:

$$I_{\beta}^{\alpha}(X_Q; Y_Q) = H_{\beta}(Y_Q) - H_{\beta}(Y_Q | X_Q)$$

Here, $H_{\beta}(Y_Q)$ represents the marginal entropy of the labels Y_Q , which is computed based on the predicted class probabilities:

$$H_{\beta}(Y_Q) = - \sum_{k=1}^K p_k^{\beta} \log p_k^{\beta}$$

Meanwhile, $H_{\beta}(Y_Q | X_Q)$ denotes the conditional entropy of the labels Y_Q given the input data X_Q :

$$H_{\beta}(Y_Q | X_Q) = \frac{1}{|Q|} \sum_{i \in Q} \sum_{k=1}^K p_{k,i}^{\beta} \log p_{k,i}^{\beta}$$

The overall loss function is formulated as:

$$L_{\text{TIM}} = \lambda \cdot CE - I_{\beta}^{\alpha}(X_Q; Y_Q)$$

where λ is a non-negative hyperparameter that balances the influence of the cross-entropy loss and the mutual information term. In our experiments, both α and λ are set to 1.

The cross-entropy loss is defined as follows:

$$CE = - \frac{1}{|Q|} \sum_{i \in Q} \sum_{k=1}^K y_{k,i} \log(p_{k,i})$$

where $y_{k,i}$ is 1 if the i -th sample belongs to class k , and 0 otherwise. By incorporating mutual information, the TIM loss helps the model capture more informative features from the input data, thereby improving both generalization and robustness.

Model evaluation

To evaluate the model's performance, we adopted common metrics, including Accuracy (ACC), Balanced Accuracy (BACC), Sensitivity (Sn), Specificity (Sp), Matthews Correlation Coefficient (MCC), Area Under the Receiver Operating Characteristic Curve (ROC AUC), and Area Under the Precision-Recall Curve (PR AUC). These metrics are calculated based on the number of True Positives (TP), False Positives (FP), False Negatives (FN), and True Negatives (TN). The formulas are as follows:

$$\text{ACC} = \frac{TP + TN}{TP + TN + FP + FN}$$

$$\text{Sn} = \frac{TP}{TP + FN}$$

$$\text{Sp} = \frac{TN}{TN + FP}$$

$$\text{BACC} = 0.5 \times \text{Sn} + 0.5 \times \text{Sp}$$

$$\text{MCC} = \frac{(TP \times TN) - (FN \times FP)}{\sqrt{(TP + FN) \times (TN + FP) \times (TP + FP) \times (TN + FN)}}$$

The Area Under the ROC Curve (ROC AUC) represents the performance of a binary classification model by plotting the true positive rate (TPR) against the false positive rate (FPR) at various threshold settings. The ROC curve shows the trade-off between sensitivity and specificity. The AUC score is the area under this curve, and it ranges from 0 to 1, where 1 indicates perfect classification and 0.5 represents random guessing. The ROC AUC is calculated using the `roc_auc_score` function from scikit-learn, which integrates the area under the ROC curve using the trapezoidal rule:

$$\text{AUC} = \int_0^1 \text{TPR}(\text{FPR}) d(\text{FPR})$$

The Area Under the Precision-Recall Curve (PR AUC) measures the trade-off between precision and recall for different

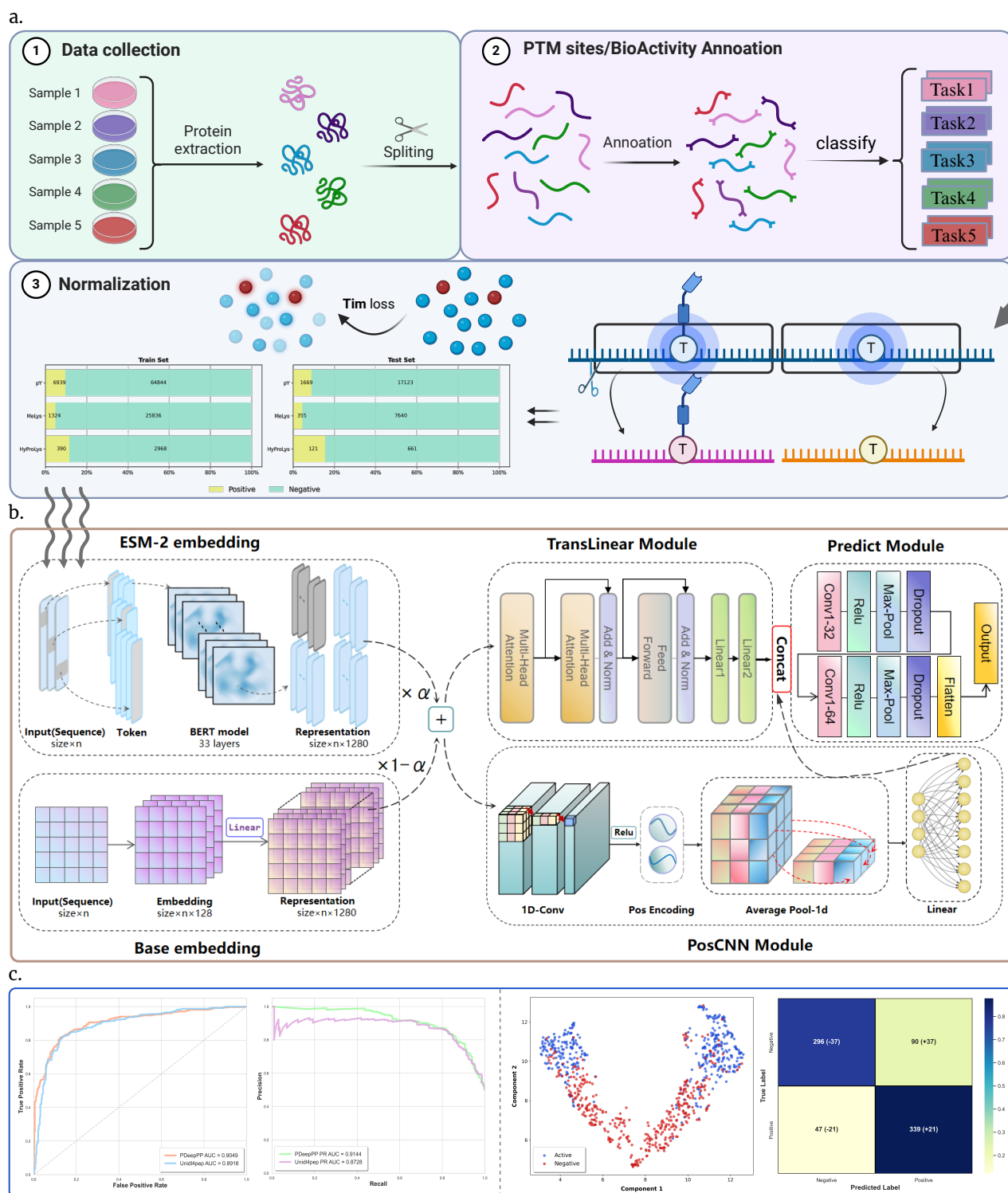


Fig. 1. The PDeepPP model usage process consists of three parts: (a) Protein extraction and trimming, peptide chain annotation with task classification, and segment trimming centered on the target amino acid with positive and negative sample classification based on site type. Special loss functions are applied to handle imbalanced datasets. (b) The model framework integrates protein-specific ESM-2 embeddings with a basic tokenizer and weighted linear layers, followed by a parallel network for global and local feature fusion, and convolutional layers for binary classification. (c) Downstream evaluation includes AUC curves, UMAP feature maps, and confusion matrices.

threshold values. Precision is defined as the proportion of true positives among all positive predictions, while recall (or sensitivity) is the proportion of true positives among all actual positives. PR AUC is particularly useful for imbalanced datasets, where the number of negatives far exceeds the number of positives. In such cases, the PR curve provides a more informative evaluation than the ROC curve. The PR AUC is computed using the ‘average_precision_score’ function in scikit-learn, which calculates the weighted mean of precision scores at each threshold:

$$\text{PR AUC} = \int_0^1 \text{Precision}(\text{Recall}) d(\text{Recall})$$

A higher PR AUC indicates better performance, particularly in imbalanced classification problems.

Results

Comparison Experiments

After normalizing the datasets, we trained each task using `esm_ratio` values of 0.9, 0.95, and 1, along with `lambda_` values ranging from 0.9 to 1 (with a step size of 0.1). The model with the best performance, determined based on ACC, AUC, and PR metrics, was selected as the optimal configuration for this experiment.

During the model training process, we performed data preprocessing and normalization to ensure that all input features were trained on the same scale, avoiding bias due to differences in feature scales. To maximize model performance, we meticulously tuned several hyperparameters and selected the optimal combination to ensure the reliability and reproducibility of the experimental results.

We accessed the UniDL4BioPep model’s server to obtain results on the same benchmark dataset. The experiments showed that, compared with the UniDL4BioPep model, our model’s ACC, AUC, and PR were on average higher by 0.3%, 0.7%, and 0.8%. Furthermore, the FN and FP were reduced by 76 and 14 samples. On the ten datasets where the model performed best, our model’s ACC increased by 2%, AUC increased by 1.67%, and PR increased by 1.87%, while the FN and FP were reduced by 71 and 67 samples, respectively. The comparison of various metrics on different datasets among PDeepPP, UniDL4BioPep, and the tools compared in UniDL4BioPep is shown in SuppTable 2.

Specifically, compared with the UniDL4BioPep model, our model shows significant advantages in classification accuracy (ACC), indicating more stable and efficient performance in the overall classification task. Additionally, the improvement in AUC suggests that our model has enhanced ability to discriminate between positive and negative samples, better capturing complex patterns in the data. The improvement in the PR curve demonstrates that our model is more robust in handling imbalanced data, particularly achieving better predictive performance for minority classes (such as positive samples). The ROC and PR curves and confusion matrices for all tasks are shown in Figure 2 and SuppFig 1.

In terms of false negatives (FN) and false positives (FP), our model also demonstrates superior performance. The reduction in FN and FP indicates that our model makes more cautious classification decisions, particularly in the test set’s positive and negative samples, effectively reducing the number of misclassifications. Specifically, the reduction in FN means that the model is more accurate in identifying positive samples,

while the reduction in FP suggests more reliable predictions for negative samples.

In the comparison with the MusiteDeep model, we also used the same benchmark dataset. The results indicate that, compared with the MusiteDeep model, our model’s ACC, AUC, and PR were on average higher by 3.3%, 0.1%, and 1.9%. Additionally, FN increased by 1,111, while FP decreased by 4,754 samples. On the six datasets where the model performed best, our model’s ACC increased by 0.8%, AUC increased by 5.0%, and PR increased by 1.6%. Even if FN increased by 3,096, FP decreased by 21,436. This indicates that the model demonstrates a significantly stronger capability in identifying negative samples on the highly imbalanced dataset, but it also leads to a deficiency in recognizing positive samples. The comparison of various metrics on different datasets between PDeepPP and MusiteDeep is shown in SuppTable 3.

In terms of classification accuracy (ACC), our model outperforms the MusiteDeep model, indicating higher stability and effectiveness in the overall classification task. The improvements in AUC and PR further suggest that our model has enhanced ability to distinguish between positive and negative samples, better adapting to different data distributions. Moreover, the improvement in the PR curve also demonstrates the advantage of our model in handling imbalanced data, particularly showing stronger sensitivity and accuracy in dealing with positive samples. The ROC and PR curves and confusion matrices for all tasks are shown in Figure 3 and SuppFig 2.

Similarly, in terms of the reduction in FN and FP, our model outperforms the MusiteDeep model. The reduction in FN and FP means that our model is more accurate in identifying positive samples and predicting negative samples, effectively avoiding misclassifications. Particularly in predicting negative samples, our model demonstrates significant advantages in terms of FP, which indicates that the risk of misclassifying negative samples as positive in practical applications will be greatly reduced.

For a comparison of the top 10 datasets from UniDL, the top 6 datasets from MusiteDeep, and the average metrics across all datasets, please refer to Figure 4.

Feature Extraction Analysis

1. Introduction to ESM Feature Extraction

ESM (Evolutionary Scale Modeling) is a large-scale protein language model based on the Transformer architecture and trained with masked language modeling on massive protein sequences from the UniRef database. By leveraging relative positional embeddings and multi-head self-attention, ESM captures evolutionary information and models amino acid interactions to generate high-dimensional representations that encode secondary and tertiary structural features. With up to 15 billion parameters, ESM-2 achieves significant improvements in perplexity and structure prediction accuracy, demonstrating strong correlations between language model understanding and atomic-level structure prediction. Its embeddings serve as inputs for ESMFold, enabling rapid and accurate end-to-end protein structure prediction without relying on MSAs, offering a computationally efficient alternative to traditional methods.

In this study, due to ESM’s specificity for proteins, ESM is utilized as the primary feature extraction tool, and the generated protein sequence embeddings are further applied to downstream analysis tasks. The core idea of feature extraction relies on the deep understanding of sequences by

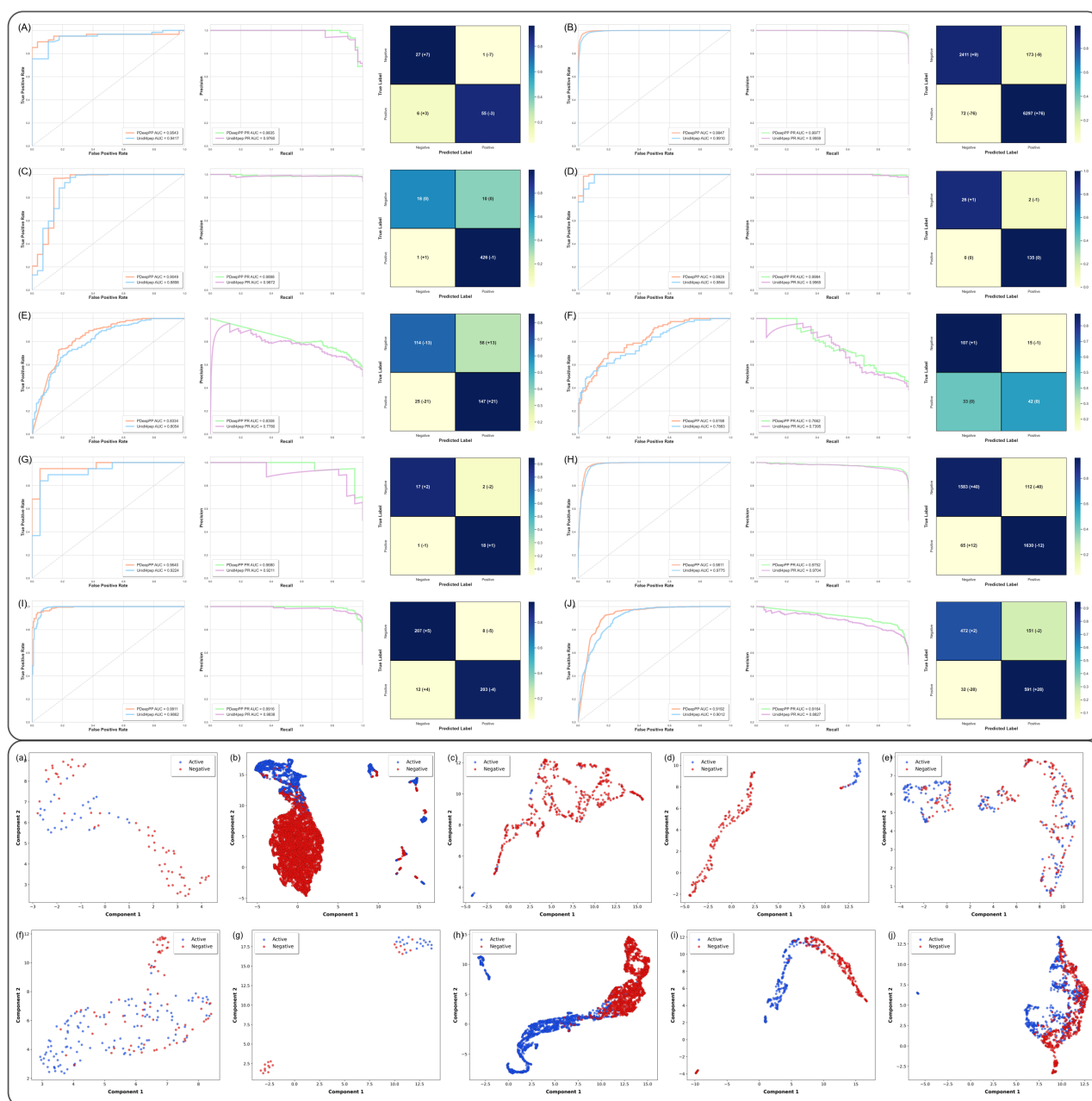


Fig. 2. The top ten tasks with the best performance in comparison with the UniDL4BioPep model. The upper section shows the AUC curves and confusion matrix combinations for each task. In the confusion matrices, the numbers in parentheses next to the values represent the difference in the count of this metric compared to PDeepPP for the UniDL4BioPep model. The color intensity of each block in the matrix indicates the proportion of that class relative to the total negative/positive samples. The lower section displays the UMAP plots for each dataset after feature extraction by PDeepPP. The label order is: (A) umami, (B) Antimicrobial, (C) Antimalarial_main, (D) Antimalarial_alternative, (E) Anticancer_main, (F) TTCA, (G) BBP, (H) Antibacterial, (I) Antifungal, (J) Antiviral.

the ESM model, thereby providing biologically meaningful representations for downstream tasks. We adopt the residual connection strategy by adding an embedding layer based on linear transformations and perform weighted feature extraction to enhance representation capacity, optimizing the performance of downstream tasks.

2. UMAP Visualization of Model Features

In this study, UMAP (Uniform Manifold Approximation and Projection) is utilized to visualize the high-dimensional embeddings extracted before the prediction module(72; 73). (UMAP is a nonlinear dimensionality reduction technique that projects high-dimensional data into a two-dimensional space, enabling intuitive observation of data distribution and clustering patterns.) These embeddings are derived from the combined outputs of the TransLinear layer and the PosCNN layer, averaged along the sequence dimension. From the UMAP

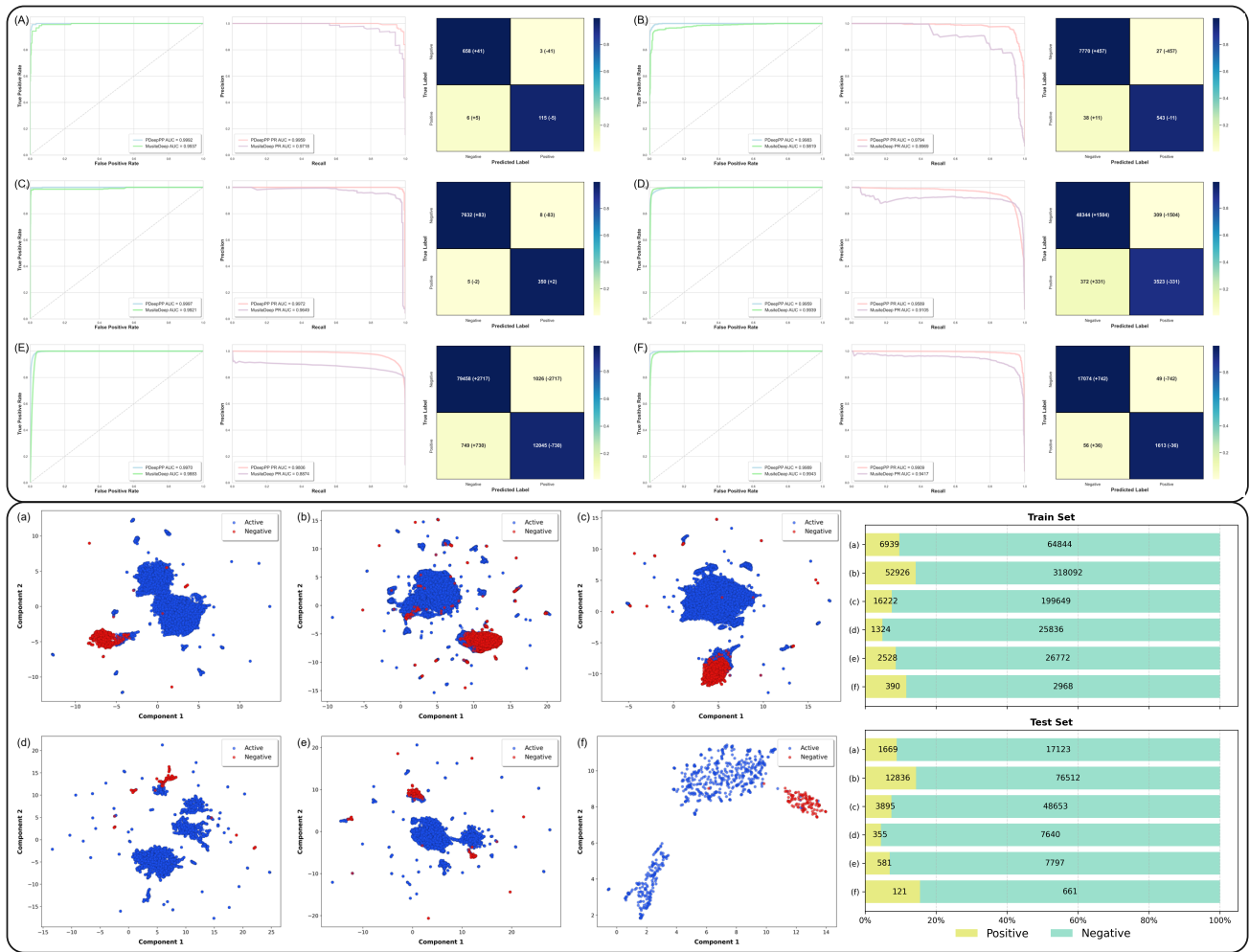


Fig. 3. The top six tasks with the best performance in comparison with the MusiteDeep model. The upper section shows the AUC curves and confusion matrix combinations for each task. In the confusion matrices, the numbers in parentheses next to the values represent the difference in the count of this metric compared to PDeepPP for the MusiteDeep model. The color intensity of each block in the matrix indicates the proportion of that class relative to the total negative/positive samples. The lower section displays the UMAP plots after feature extraction by PDeepPP, with the site distribution of these six datasets shown in the bottom right. The label order is: (A) Phosphorylation_Y, (B) N-linked-glycosylation_N, (C) N6-acetyllysine_K, (D) Methylation_K, (E) Ubiquitin_K, (F) Hydroxyproline_K.

visualization, it can be observed that the features generated by the model exhibit effective class separation after dimensionality reduction, with distinct clusters formed in the reduced feature space for different categories.

By visualizing with UMAP, researchers can intuitively observe the clustering patterns and inter-class differences of different protein features, providing important insights into the interpretability of the model and the relationships between features. The UMAP visualization of the UniDL4BioPep dataset shows clear clustering trends for different categories. This indicates that the features extracted by the model have strong discriminative power. The specific analysis is as follows:

3. Analysis of UniDL4BioPep UMAP Visualization

(Figure 2 and SuppFig 1)

Cluster Distribution and Category Separation

- In Figure 1 (a), (b), (h), and (i), the red and blue points are clearly separated with distinct clusters, indicating good category separation.
- In Figure 1 (c), the red and blue points show some overlap, with the clusters less tight, suggesting weaker category separation.
- In Figure 1 (d), (f), and (j) and Figure 2 (d), (f), and (j), the red and blue points heavily overlap, indicating poor category separation and suggesting that the model struggles to distinguish between the categories.

Boundary Clarity and Overlap

- In Figure 1 (a), (b), (h), and (i) and Figure 2 (a), (b), (h), and (i), the boundaries are clear, and there is minimal overlap between the categories.
- In Figure 1 (c) and Figure 2 (c), the boundaries are somewhat blurred with noticeable overlap, leading to less effective category separation.

- In **Figure 1 (d), (f), and (j)** and **Figure 2 (d), (f), and (j)**, the red and blue points overlap significantly, with unclear boundaries, making it difficult to distinguish between categories.

Outlier Distribution

- In **Figure 1 (a), (b), and (h)** and **Figure 2 (a), (b), and (h)**, there are few outliers, and they are evenly distributed, having minimal impact on clustering.
- In **Figure 1 (c)** and **Figure 2 (i)**, there are more noticeable outliers, which may affect clustering performance and category separation.

Category Overlap

- In **Figure 1 (d), (f), and (j)** and **Figure 2 (d), (f), and (j)**, there is significant overlap between categories, making it difficult for the model to distinguish between the red and blue classes.

4. Analysis of MusiteDeep UMAP Visualization (Figure 3 and SuppFig 2)

Cluster Distribution and Category Separation

In **Figure 1** and **Figure 2**, the distribution of blue (Active) and red (Negative) points demonstrates different clustering characteristics. **Figure 1(a)** and **Figure 1(d)** show clear category separation, with blue points clustered tightly while red points are fewer and primarily located at the edges of the blue clusters. In contrast, **Figure 1(b)** and **Figure 1(e)** exhibit more overlap between blue and red points, particularly at the edges of the clusters.

Boundary Clarity and Overlap

The clarity of boundaries varies across the figures. In **Figure 1(a)** and **Figure 1(d)**, the boundaries between blue and red points are very clear, with minimal overlap. **Figure 1(b)** and **Figure 1(c)** show more blurred boundaries, with some red points clearly overlapping blue points, while **Figure 1(f)** presents a long, narrow cluster of blue points, with red points mainly concentrated at the edges.

Outlier Distribution

The distribution of outliers also differs among the figures. **Figure 1(a)** and **Figure 1(d)** contain a small number of red outliers, whereas **Figure 1(b)** and **Figure 1(c)** show an increased number of red outliers, predominantly located at the edges of the blue points. In **Figure 1(f)**, the number of red points is sparse, with outliers mainly surrounding the blue points.

Ablation Study

In this subsection, we conduct an ablation study to evaluate the contribution of key modules in our model(74). By systematically removing specific components, we analyze the impact on performance using ROC/PR curves, confusion matrices, and UMAP visualizations.

Dataset Selection

For dataset selection, we first chose four datasets from the UniDL4BioPep and MusiteDeep collections based on dataset size, the ratio of positive to negative sites, and prediction performance. These included Anticancer_main and Antiviral from UniDL4BioPep, and N6-acetyllysine.K and Ubiquitin.K from MusiteDeep, which served as the first batch of datasets for the ablation study. To explore the model's performance on tasks

with additional classification targets, similar post-translational modification (PTM) types with emphasis on different amino acids, and tasks where both PTM type and target amino acid are the same, we selected several recent state-of-the-art (SOTA) datasets from recent literature. These datasets include methylation-G(60), methylation-R (distinguished from the corresponding task in MusiteDeep by the lowercase letter)(61), Ubiquitin.K* (the asterisk is used to differentiate it from the corresponding task in MusiteDeep)(62), and Crotonylation_K(63). The goal of this selection is to verify the model's robustness and completeness by testing it on diverse datasets while ensuring that each module contributes positively to the overall model performance. The specific sample sizes and the distribution of negative and positive samples across datasets (especially for imbalanced datasets) are shown in SuppTable 1 and Figure 5, respectively.

Experimental Setup

We design several ablation experiments:

- Full model (baseline).
- Removing pre-trained embeddings (sequence or structure).
- Replacing the TIM loss function with a standard cross-entropy loss.
- Removing the PosCNN(&PosEncoding) or TransLinear(&First attention layer) module.

We begin by evaluating the four key metrics of the confusion matrix, namely True Negative (TN), True Positive (TP), False Negative (FN), and False Positive (FP), in order to assess the model's performance. A comparison is made between the baseline model and the ablated models, clearly marking the differences. Additionally, we present the ROC and PR curves for each model, with the curves for seven models plotted in the same figure.

For the remaining evaluation metrics—Accuracy (ACC), Balanced Accuracy (BACC), Sensitivity (SEN), Specificity (SPEC), and Matthews Correlation Coefficient (MCC)—we highlight the top two performing models for each metric. The best model is marked in red, and the second-best model in blue. The results of these three evaluation methods are shown in Figure 5.

In the next step, we visualize the UMAP projections of the seven models, categorizing them into three distinct groups, as follows:

$$\text{Categories} = \begin{bmatrix} [\text{PDeepPP, w/o embedding, w/o loss}], \\ [\text{PDeepPP, w/o attention, w/o Translinear}], \\ [\text{PDeepPP, w/o PosEncoding, w/o PosCNN}] \end{bmatrix}$$

These categories are organized based on related modules and their comparison to the baseline model. Finally, we compute the average performance metrics across the eight datasets for both the baseline and ablated models. These results are visualized in the laser bar chart presented in Figure 6 and SuppFig 3.

Results and Analysis

1. ROC/PR Curves

The full model demonstrates strong performance across all tasks, with median AUC of 0.991 (80% of tasks achieving AUC between 0.982-0.998). Key observations:

- Removing sequence embeddings causes 9.7% AUC drop (from 0.985 to 0.890) in PTM predictions
- Structure embedding removal shows smaller impact (3.2% average AUC decrease)
- Dual component removal leads to maximum 12.7%

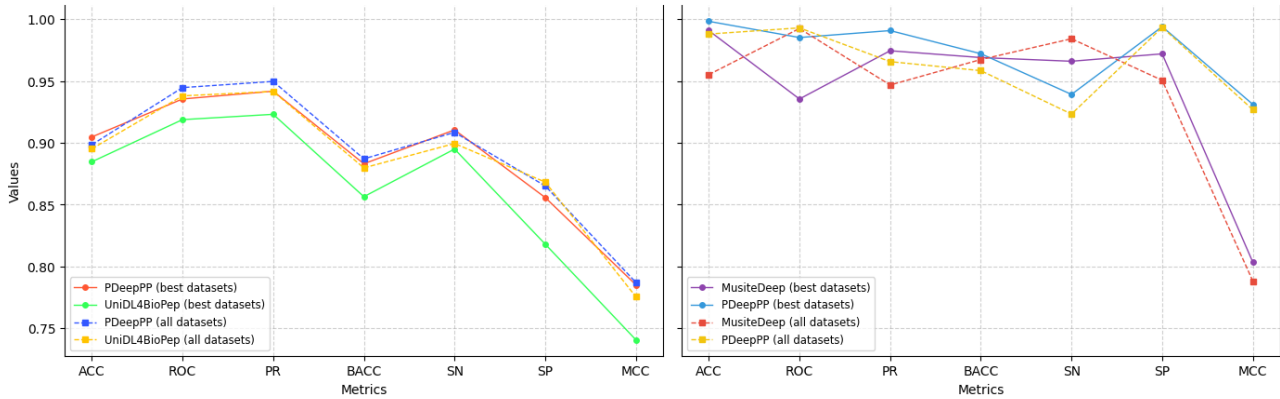


Fig. 4. The best-performing datasets in comparison with the UniDL4BioPep and MusiteDeep models (10 datasets for UniDL4BioPep and 6 for MusiteDeep) and the average values of metrics across all datasets.

performance reduction

2. Confusion Matrix

Component removal creates distinct error patterns:

- Missing CNN increases false alarms by $2.1\times$ (e.g., antimicrobial detection: $84\rightarrow 176$ cases), which suggests that the CNN module plays a critical role in filtering out incorrect predictions
- Losing Transformer raises missed detections by 37.5% (anticancer task: $152\rightarrow 209$ cases), highlighting the importance of this module in correctly identifying positive instances.
- Positional encoding removal causes combined degradation (both error types increasing over 100%)

This behavior is consistent across different datasets, as indicated by the confusion matrix behavior for each ablation variant.

3. UMAP Visualization: As depicted in Figure 6& SuppFig 3, the UMAP projections clearly show that the full model achieves superior separation between positive and negative samples in the feature space. In contrast, removing embeddings or key modules results in overlapping distributions, demonstrating a reduction in the model’s ability to discriminate between the classes.

- Average distance between categories: 1.73 vs 0.91 in others
- Category differentiation improved by 29%
- Decision boundaries $3\times$ clearer

These advantages enable 6.8% better accuracy on challenging cases.

4. Average Performance Metrics In this part of the analysis, we focus on the performance of different models across multiple evaluation metrics. By comparing the baseline model (PDeepPP) and the six ablation variants on average values for each metric, we can better understand the contribution of each key module.

First, **Accuracy (ACC)** and **Balanced Accuracy (BACC)** exhibit similar trends. From the table, we see that the baseline model (PDeepPP) achieves the highest scores for these two metrics, 0.8349 and 0.8282, respectively. Removing the embedding module results in almost the same performance as the baseline, indicating that embeddings have a minimal effect on these metrics. However, after removing the attention mechanism and translinear layer, both metrics show a noticeable decline, particularly BACC, with scores of 0.8267 and 0.8359, slightly lower than the baseline. This suggests that

the attention mechanism and translinear layer play a significant role in improving model performance.

For **Sensitivity (SN)** and **Specificity (SP)**, the baseline model and the embedding-removed model have identical scores, indicating that the embedding module has a relatively mild impact on these metrics. Removing the CNN module results in a reduction in sensitivity (0.7915), while specificity remains at a relatively high level (0.8301). This indicates that removing the CNN module increases false negatives (FN), affecting the model’s ability to recognize positive samples. In contrast, removing the Transformer module leads to an increase in false positives (FP), resulting in a higher specificity but a more significant decline in sensitivity.

Matthews Correlation Coefficient (MCC) shows a similar trend. The MCC value for the baseline model (PDeepPP) is 0.8265, the highest among all models. The models without embeddings and without CNN modules follow closely, with scores of 0.8265 and 0.8089, respectively. In contrast, removing the PosEncoding and PosCNN modules results in a substantial drop in MCC values, 0.6511 and 0.5503, respectively, indicating that removing these modules severely affects the model’s overall performance.

Overall, the baseline model (PDeepPP) performs best across all metrics, while removing the embedding module has the least effect on performance. On the other hand, removing PosEncoding and PosCNN leads to the most significant performance degradation. In particular, removing PosEncoding and PosCNN not only reduces accuracy but also significantly affects sensitivity and MCC, indicating that they play a critical role in the model.

Conclusion

The PDeepPP framework represents a significant leap forward in the field of peptide classification and PTM prediction, showcasing the transformative power of deep learning in addressing complex bioinformatics challenges. Our experimental results demonstrate that PDeepPP consistently outperforms state-of-the-art models across a variety of tasks, underscoring its robustness and adaptability. For instance, in antimicrobial peptide classification, PDeepPP achieved an impressive accuracy (ACC) of 0.9726 and a PR AUC of 0.9977, significantly surpassing the performance of UniDL4BioPep. Similarly, in phosphorylation site prediction, a critical PTM

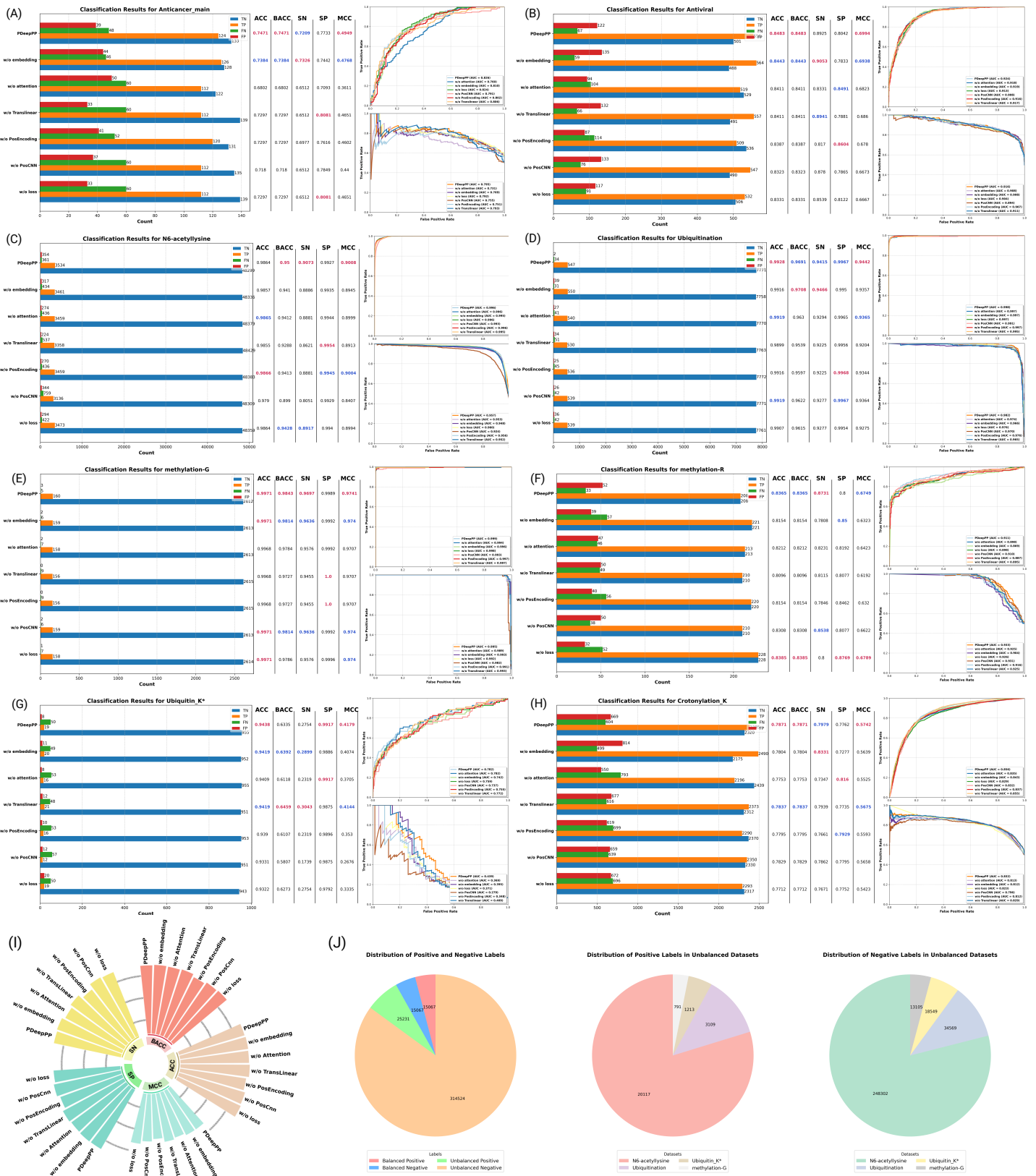


Fig. 5. (A)-(H) show the classification results of PDeepPP and six ablated models on the tasks: Anticancer_main, Antiviral, N6-acetylysine, Ubiquitination, methylation-G, methylation-R, Ubiquitin K*, and Crotonylation.K. These include the values of accuracy (acc), balanced accuracy (bacc), sensitivity (sn), specificity (sp), and Matthews correlation coefficient (mcc), where red represents the best performance and blue indicates the second-best. The results also include the ROC and PR curves. (I) presents the average values of acc, bacc, sn, sp, and mcc across all datasets for these seven models. (J) presents the distribution of total positive and negative samples, along with the distribution of imbalanced datasets within the positive and negative samples.

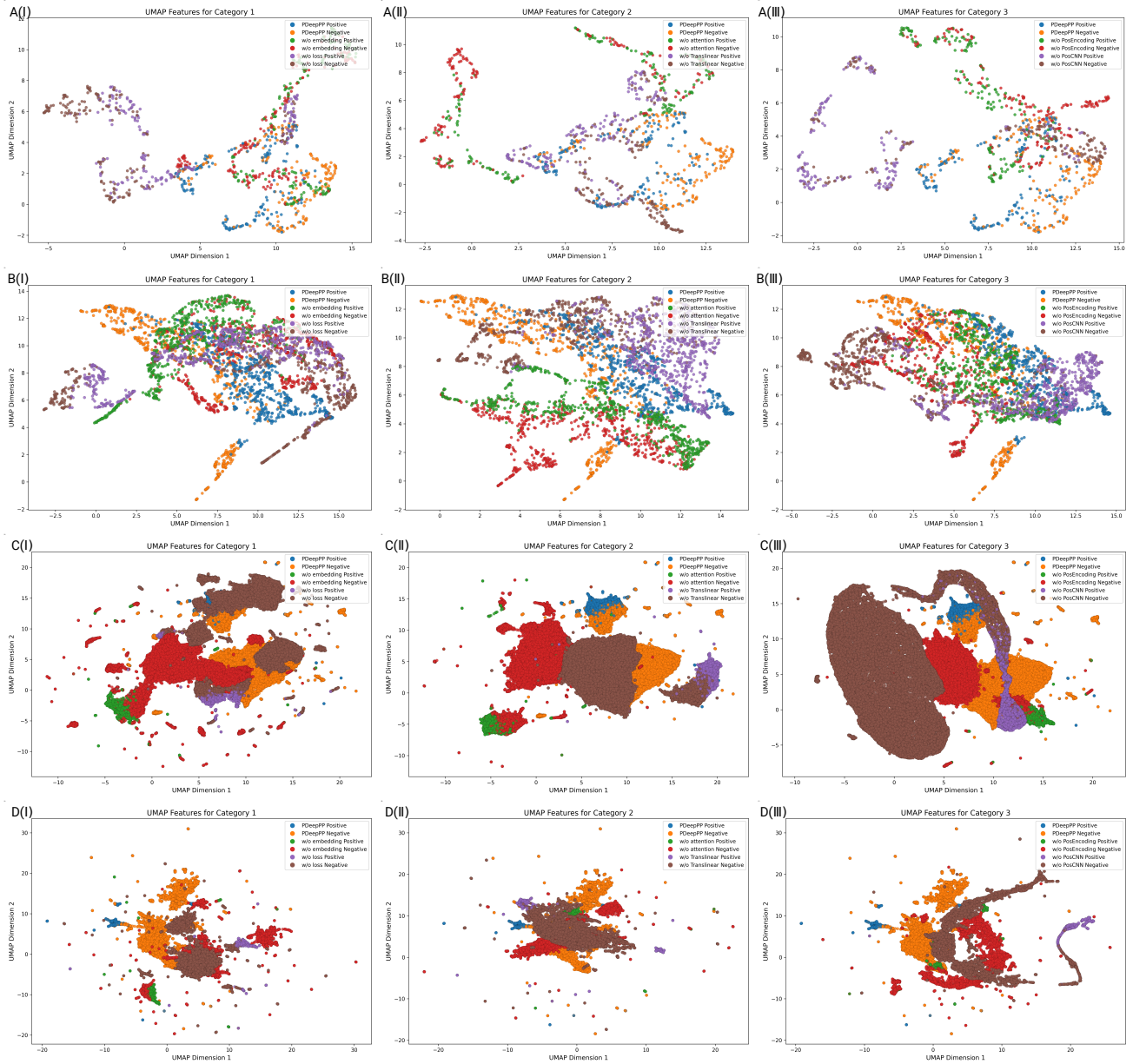


Fig. 6. Four datasets selected from existing categories, with respect to the given category (see legend). UMAP plots are shown for each pair of related ablated models and the baseline model (PDeepPP) after feature extraction. (A)-(D) correspond to Anticancer_main, Antiviral, N6-acetyllysine, and Ubiquitination, respectively.

task, PDeepPP achieved an ACC of 0.9984 and a PR AUC of 0.9910, highlighting its exceptional predictive capabilities and ability to generalize across diverse datasets. Furthermore, PDeepPP substantially reduced false positives (FP) and false negatives (FN) across all tested datasets, reinforcing its practical utility in real-world applications.

PDeepPP's success can be attributed to its innovative integration of pretrained protein language models (ESM-2) with a parallel neural network architecture combining Transformers and CNNs. This design allows the model to capture both local and global sequence features, enhancing its ability to handle the complexity of protein sequences. The inclusion of the Transductive Information Maximization (TIM) loss function further improves performance on imbalanced datasets,

a common challenge in bioinformatics. This combination of advanced deep learning techniques enables PDeepPP to achieve superior accuracy, robustness, and scalability compared to traditional methods.

Compared to conventional models, PDeepPP significantly reduces the need for extensive feature engineering and manual annotation, making it adaptable to a wide range of PTM types and peptide functionalities. Its ability to handle large-scale datasets and diverse biological tasks positions it as a valuable tool for large-scale bioinformatics research. Moreover, PDeepPP's computational efficiency and reduced reliance on experimental data make it a cost-effective solution for peptide discovery and PTM analysis.

Looking ahead, PDeepPP holds immense potential for broader applications in both research and industry. Future directions include integrating structural and spatial data to further enhance predictive accuracy, as well as combining the framework with high-throughput experimental workflows to accelerate large-scale protein function discovery and drug development. Additionally, as novel PTM types, such as AMPylation, are discovered, PDeepPP can provide computational support for exploring these uncharted areas, advancing its potential applications in precision medicine and therapeutic innovation. The framework could also be extended to address multi-label classification tasks, where peptides may exhibit multiple bioactivities or PTMs simultaneously, further broadening its utility.

In summary, PDeepPP combines the strengths of pretrained protein language models, advanced neural network architectures, and innovative loss functions to offer a cutting-edge solution for protein sequence analysis. It represents a major advancement in the field of bioinformatics and has the potential to play a pivotal role in accelerating peptide discovery, PTM functional analysis, and the development of novel therapeutic strategies. By reducing the reliance on costly and time-consuming experimental methods, PDeepPP not only enhances the efficiency of bioinformatics research but also opens new avenues for understanding the complex mechanisms underlying protein modifications and peptide bioactivity. As the field continues to evolve, PDeepPP is poised to drive innovation in life sciences, contributing to the development of targeted therapies and personalized medicine.

References

- Hasan Zulfqar, Zhiling Guo, Ramala Masood Ahmad, Zahoor Ahmed, Peiling Cai, Xiang Chen, Yang Zhang, Hao Lin, and Zheng Shi. Deep-stp: a deep learning-based approach to predict snake toxin proteins by using word embeddings. *Frontiers in Medicine*, 10:1291352, 2024.
- Wireko Andrew Awuah, Adam Ben-Jaafar, Subham Roy, Princess Afia Nkrumah-Boateng, Joecelyn Kirani Tan, Toufik Abdul-Rahman, and Oday Atallah. Predicting survival in malignant glioma using artificial intelligence. *European Journal of Medical Research*, 30(1):61, 2025.
- Lantian Yao, Peilin Xie, Danhong Dong, Yilin Guo, Jiahui Guan, Wenyang Zhang, Chia-Ru Chung, Zhihao Zhao, Ying-Chih Chiang, and Tzong-Yi Lee. Caps-ac4c: an effective computational framework for identifying n4-acetylcytidine sites in human mrna based on deep learning. *Journal of Molecular Biology*, page 168961, 2025.
- Radha G. Krishna and Finn Wold. *Post-Translational Modification of Proteins*, pages 265–298. John Wiley & Sons, Ltd, 1993.
- Shahin Ramazi and Javad Zahiri. Post-translational modifications in proteins: resources, tools and prediction methods. *Database*, 2021:baab012, 04 2021.
- Swatika Prabakaran, Guy Lippens, Hanno Steen, and Jeremy Gunawardena. Post-translational modification: nature's escape from genetic imprisonment and the basis for dynamic information encoding. *Wiley Interdisciplinary Reviews: Systems Biology and Medicine*, 4(6):565–583, Nov-Dec 2012. Epub 2012 Aug 15.
- Kuldeep Singh, Jeetendra Kumar Gupta, Aman Shrivastava, Divya Jain, Amrendra Pratap Yadav, Sumeet Dwivedi, Anubhav Dubey, and Shivendra Kumar. Exploring the pharmacological effects of bioactive peptides on human nervous disorders: A comprehensive review. *CNS & Neurological Disorders - Drug Targets (Formerly Current Drug Targets - CNS & Neurological Disorders)*, 24(1):32–46, 2025.
- Zhenjiao Du and Yonghui Li. Review and perspective on bioactive peptides: A roadmap for research, development, and future opportunities. *Journal of Agriculture and Food Research*, 9:100353, 2022.
- Ruann Janser Soares de Castro and Hélia Harumi Sato. Biologically active peptides: Processes for their generation, purification and identification and applications as natural additives in the food and pharmaceutical industries. *Food Research International*, 74:185–198, 2015.
- Ahmed A Zaky, Jesus Simal-Gandara, Jong-Bang Eun, Jae-Han Shim, and AM Abd El-Aty. Bioactivities, applications, safety, and health benefits of bioactive peptides from food and by-products: A review. *Frontiers in Nutrition*, 8:815640, 2022.
- Philip Cohen. The role of protein phosphorylation in human health and disease. *European Journal of Biochemistry*, 268(19):5001–5010, 2001.
- Kazuaki Ohtsubo and Jamey D. Marth. Glycosylation in cellular mechanisms of health and disease. *Cell*, 126(5):855–867, 2006. doi: 10.1016/j.cell.2006.08.019.
- Tony Kouzarides. Acetylation: a regulatory modification to rival phosphorylation? *The EMBO Journal*, 19(6):1176–1179, 2000.
- Tejaswita M. Karve and Amrita K. Cheema. Small changes huge impact: The role of protein posttranslational modifications in cellular homeostasis and disease. *Journal of Amino Acids*, 2011(1):207691, 2011.
- Fereidoon Shahidi and Ying Zhong. Bioactive peptides. *Journal of AOAC INTERNATIONAL*, 91(4):914–931, 11 2019.
- Dora Elisa Cruz-Casas, Cristóbal N Aguilar, Juan A Ascacio-Valdés, Raúl Rodríguez-Herrera, Mónica L Chávez-González, and Adriana C Flores-Gallegos. Enzymatic hydrolysis and microbial fermentation: The most favorable biotechnological methods for the release of bioactive peptides. *Food Chemistry: Molecular Sciences*, 3:100047, 2021.
- Leticia Mora and Fidel Toldrá. Advanced enzymatic hydrolysis of food proteins for the production of bioactive peptides. *Current Opinion in Food Science*, 49:100973, 2023.
- Lauren Elizabeth Smith and Adelina Rogowska-Wrzesinska. The challenge of detecting modifications on proteins. *Essays in Biochemistry*, 64(1):135–153, 01 2020.
- Ivan Verrastro, Sabah Pasha, Karina Tveen Jensen, Andrew R. Pitt, and Corinne M. Spickett. Mass spectrometry-based methods for identifying oxidized proteins in disease: Advances and challenges. *Biomolecules*, 5(2):378–411, 2015.
- Min-Sik Kim, Jun Zhong, and Akhilesh Pandey. Common errors in mass spectrometry-based analysis of post-translational modifications. *PROTEOMICS*, 16(5):700–714, 2016.
- Piotr Minkiewicz, Jerzy Dziuba, Anna Iwaniak, Marta Dziuba, and Magorzata Darewicz. Biopep database and other programs for processing bioactive peptide sequences. *Journal of AOAC INTERNATIONAL*, 91(4):965–980, 11 2019.

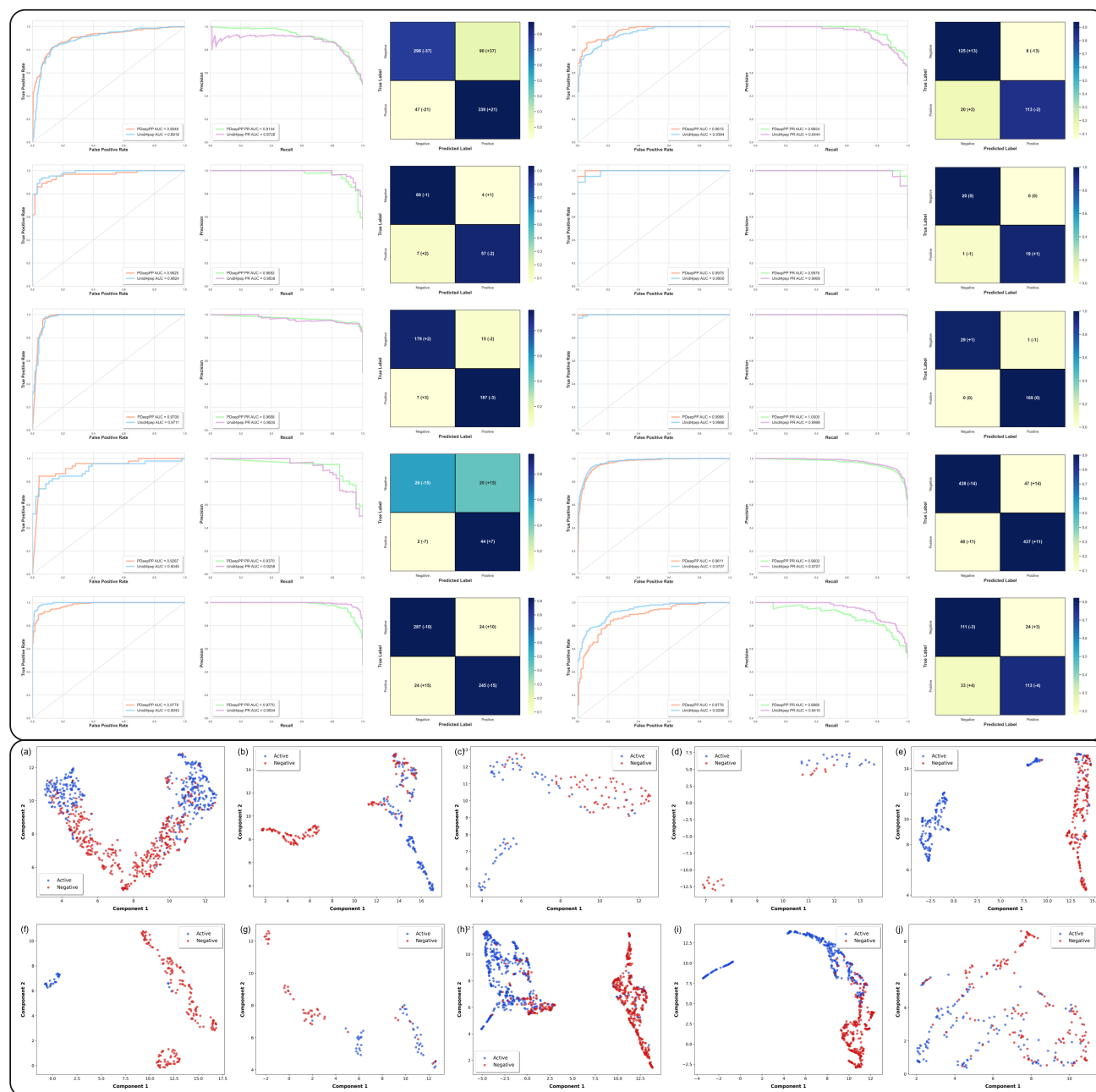
22. Alice B. Nongonierma and Richard J. FitzGerald. Strategies for the discovery and identification of food protein-derived biologically active peptides. *Trends in Food Science & Technology*, 69:289–305, 2017. Food Bioactives: From evidence of health benefits to understanding mechanisms.
23. Duolin Wang, Dongpeng Liu, Jiakang Yuchi, Fei He, Yuexu Jiang, Siteng Cai, Jingyi Li, and Dong Xu. Musitedeep: a deep-learning based webserver for protein post-translational modification site prediction and visualization. *Nucleic Acids Research*, 48(W1):W140–W146, 04 2020.
24. Jian Gao, Jay J. Thelen, A. Keith Dunker, and Dong Xu. Musite, a tool for global prediction of general and kinase-specific phosphorylation sites. *Molecular & Cellular Proteomics*, 9(12):2586–2600, Dec 2010. Epub 2010 Aug 11.
25. De-Shuang Wang, Sha Zeng, Chao Xu, Wei Qiu, Yong Liang, Trupti Joshi, and Dong Xu. Musitedeep: a deep-learning framework for general and kinase-specific phosphorylation site prediction. *Bioinformatics*, 33(24):3909–3916, Dec 2017.
26. De-Shuang Wang, Yong Liang, and Dong Xu. Capsule network for protein post-translational modification site prediction. *Bioinformatics*, 35(14):2386–2394, Jul 2019.
27. Zhenjiao Du, Xingjian Ding, Yixiang Xu, and Yonghui Li. Unid4biopep: a universal deep learning architecture for binary classification in peptide bioactivity. *Briefings in Bioinformatics*, 24(3):bbad135, 04 2023.
28. Ziyang Xu and Haitian Zhong. Ptransips: Identification of phosphorylation sites based on protein pretrained language model and transformer. *ArXiv*, abs/2308.05115, 2023.
29. Thi-Xuan Tran, Nguyen Quoc Khanh Le, and Van-Nui Nguyen. Integrating cnn and bi-lstm for protein succinylation sites prediction based on natural language processing technique. *Computers in Biology and Medicine*, 186:109664, 2025.
30. Zhaomin Yao, Fei Li, Weiming Xie, Jiaming Chen, Jiezhong Wu, Ying Zhan, Xiaodan Wu, Zhiguo Wang, and Guoxu Zhang. DeepSF-4mC: A deep learning model for predicting dna cytosine 4mC methylation sites leveraging sequence features. *Computers in Biology and Medicine*, 171:108166, 2024.
31. Bo Wen, Wen-Feng Zeng, Yuxing Liao, Zhiao Shi, Sara R. Savage, Wen Jiang, and Bing Zhang. Deep learning in proteomics. *PROTEOMICS*, 20(21-22):1900335, 2020.
32. Subash C. Pakhrin, Suresh Pokharel, Hiroto Saigo, and Dukka B. KC. *Deep Learning-Based Advances In Protein Posttranslational Modification Site and Protein Cleavage Prediction*, pages 285–322. Springer US, New York, NY, 2022.
33. Anurag S. Rathore, Saxena Nikita, Garima Thakur, and Somesh Mishra. Artificial intelligence and machine learning applications in biopharmaceutical manufacturing. *Trends in Biotechnology*, 41(4):497–510, 2023. doi: 10.1016/j.tibtech.2022.08.007.
34. Harini Narayanan, Fabian Dingfelder, Itzel Condado Morales, Bhargav Patel, Kristine Enemærke Heding, Jais Rose Bjelke, Thomas Egebjerg, Alessandro Butté, Michael Sokolov, Nikolai Lorenzen, and Paolo Arosio. Design of biopharmaceutical formulations accelerated by machine learning. *Molecular Pharmaceutics*, 18(10):3843–3853, 2021. PMID: 34519511.
35. Vivek Bhakta Mathema, Partho Sen, Santosh Lamichhane, Matej Orešič, and Sakda Khoomrung. Deep learning facilitates multi-data type analysis and predictive biomarker discovery in cancer precision medicine. *Computational and Structural Biotechnology Journal*, 21:1372–1382, 2023.
36. Zeming Lin, Halil Akin, Roshan Rao, Brian Hie, Zhongkai Zhu, Wenting Lu, Nikita Smetanin, Robert Verkuil, Ori Kabeli, Yaniv Shmueli, Allan dos Santos Costa, Maryam Fazel-Zarandi, Tom Sercu, Salvatore Candido, and Alexander Rives. Evolutionary-scale prediction of atomic-level protein structure with a language model. *Science*, 379(6637):1123–1130, 2023.
37. A Vaswani. Attention is all you need. *Advances in Neural Information Processing Systems*, 2017.
38. Y. Lecun, L. Bottou, Y. Bengio, and P. Haffner. Gradient-based learning applied to document recognition. *Proceedings of the IEEE*, 86(11):2278–2324, 1998.
39. José Dolz, Pablo Piantanida, and Ismail Ben Ayed. Transductive information maximization for few-shot learning, 2020.
40. Mateusz Buda, Atsuto Maki, and Maciej A Mazurowski. A systematic study of the class imbalance problem in convolutional neural networks. *Neural networks*, 106:249–259, 2018.
41. Balachandran Manavalan, Shaherin Basith, Tae Hwan Shin, Leyi Wei, and Gwang Lee. mAHTPred: a sequence-based meta-predictor for improving the prediction of anti-hypertensive peptides using effective feature representation. *Bioinformatics*, 35(16):2757–2765, 12 2018.
42. Phasit Charoenkwan, Sakawrat Kanthawong, Chanin Nantasenamat, Md. Mehedi Hasan, and Watshara Shoombuatong. idppiv-scm: A sequence-based predictor for identifying and analyzing dipeptidyl peptidase iv (dpp-iv) inhibitory peptides using a scoring card method. *Journal of Proteome Research*, 19(10):4125–4136, 2020. PMID: 32897718.
43. Phasit Charoenkwan, Chanin Nantasenamat, Md Mehedi Hasan, Balachandran Manavalan, and Watshara Shoombuatong. BERT4Bitter: a bidirectional encoder representations from transformers (BERT)-based model for improving the prediction of bitter peptides. *Bioinformatics*, 37(17):2556–2562, 02 2021.
44. Phasit Charoenkwan, Janchai Yana, Chanin Nantasenamat, Md. Mehedi Hasan, and Watshara Shoombuatong. iumami-scm: A novel sequence-based predictor for prediction and analysis of umami peptides using a scoring card method with propensity scores of dipeptides. *Journal of Chemical Information and Modeling*, 60(12):6666–6678, 2020. PMID: 33094610.
45. Yuxuan Pang, Lantian Yao, Jingyi Xu, Zhuo Wang, and Tzong-Yi Lee. Integrating transformer and imbalanced multi-label learning to identify antimicrobial peptides and their functional activities. *Bioinformatics*, 38(24):5368–5374, 11 2022.
46. Phasit Charoenkwan, Nalini Schaduagratt, Pietro Lio, Mohammad Ali Moni, Pramote Chumnanpuen, and Watshara Shoombuatong. iamp-scm: A novel computational tool for large-scale identification of antimalarial peptides using estimated propensity scores of dipeptides. *ACS Omega*, 7(45):41082–41095, 2022.
47. Hang Wei and Bin Liu. iCircDA-MF: identification of circRNA-disease associations based on matrix factorization. *Briefings in Bioinformatics*, 21(4):1356–1367, 06 2019.
48. Piyush Agrawal, Dhruv Bhagat, Manish Mahalwal, Neelam Sharma, and Gajendra P S Raghava. AntiCP 2.0: an updated model for predicting anticancer peptides. *Briefings*

- in Bioinformatics*, 22(3):bbaa153, 08 2020.
49. Phasit Charoenkwan, Wararat Chiangjong, Vannajan Sanghiran Lee, Chanin Nantasenammat, Md. Mehedi Hasan, and Watshara Shoombuatong. Improved prediction and characterization of anticancer activities of peptides using a novel flexible scoring card method. *Scientific Reports*, 11(1):3017, 2021.
 50. Phasit Charoenkwan, Sakawrat Kanthawong, Nalini Schaduangrat, Pietro Li', Mohammad Ali Moni, and Watshara Shoombuatong. ScmrSa: a new approach for identifying and analyzing anti-mrsa peptides using estimated propensity scores of dipeptides. *ACS Omega*, 7(36):32653–32664, 2022.
 51. Phasit Charoenkwan, Chanin Nantasenammat, Md Mehedi Hasan, and Watshara Shoombuatong. ittca-hybrid: Improved and robust identification of tumor t cell antigens by utilizing hybrid feature representation. *Analytical Biochemistry*, 599:113747, 2020.
 52. Ruyu Dai, Wei Zhang, Wending Tang, Evelien Wynendaele, Qizhi Zhu, Yannan Bin, Bart De Spiegeleer, and Junfeng Xia. Bbpped: Sequence-based prediction of blood-brain barrier peptides with feature representation learning and logistic regression. *Journal of Chemical Information and Modeling*, 61(1):525–534, 2021. PMID: 33426873.
 53. Phasit Charoenkwan, Wararat Chiangjong, Vannajan Sanghiran Lee, Chanin Nantasenammat, Md. Mehedi Hasan, and Watshara Shoombuatong. Improved prediction and characterization of anticancer activities of peptides using a novel flexible scoring card method. *Scientific Reports*, 11(1):3017, 2021.
 54. Yannan Bin, Wei Zhang, Wending Tang, Ruyu Dai, Menglu Li, Qizhi Zhu, and Junfeng Xia. Prediction of neuropeptides from sequence information using ensemble classifier and hybrid features. *Journal of Proteome Research*, 19(9):3732–3740, 2020. PMID: 32786686.
 55. Shouzhi Chen, Qing Li, Jianping Zhao, Yannan Bin, and Chunhou Zheng. NeuroPred-CLQ: incorporating deep temporal convolutional networks and multi-head attention mechanism to predict neuropeptides. *Briefings in Bioinformatics*, 23(5):bbac319, 08 2022.
 56. Sergio A. Pinacho-Castellanos, César R. García-Jacas, Michael K. Gilson, and Carlos A. Brizuela. Alignment-free antimicrobial peptide predictors: Improving performance by a thorough analysis of the largest available data set. *Journal of Chemical Information and Modeling*, 61(6):3141–3157, 2021. PMID: 34081438.
 57. Lesong Wei, Xiucui Ye, Yuyang Xue, Tetsuya Sakurai, and Leyi Wei. ATSE: a peptide toxicity predictor by exploiting structural and evolutionary information based on graph neural network and attention mechanism. *Briefings in Bioinformatics*, 22(5):bbab041, 04 2021.
 58. Tobias Hegelund Olsen, Betül Yesiltas, Frederikke Isa Marin, Margarita Pertseva, Pedro J. García-Moreno, Simon Gregersen, Michael Toft Overgaard, Charlotte Jacobsen, Ole Lund, Egon Bech Hansen, and Paolo Marcantili. Anoxpepred: using deep learning for the prediction of antioxidative properties of peptides. *Scientific Reports*, 10(1):21471, 2020.
 59. Emmanuel Boutet, Dominique Lieberherr, Michael Tognolli, Michel Schneider, Preeti Bansal, Alan J. Bridge, Sylvain Poux, Lydie Bougueleret, and Ioannis Xenarios. Uniprotkb/swiss-prot, the manually annotated section of the uniprot knowledgebase: How to use the entry view. In *Methods in Molecular Biology*, volume 1374, pages 23–54. Springer, 2016.
 60. Sharaf J. Malebary, Ebraheem Alzahrani, and Yaser Daanial Khan. A comprehensive tool for accurate identification of methyl-glutamine sites. *Journal of Molecular Graphics and Modelling*, 110:108074, 2022.
 61. Favorisen Rosyking Lumbanraja, Bharuno Mahesworo, Tjeng Wawan Cenggoro, Digdo Sudigyo, and Bens Pardamean. Ssmfn: a fused spatial and sequential deep learning model for methylation site prediction. *PeerJ Computer Science*, 7:e683, 2021.
 62. Fei He, Jingyi Li, Rui Wang, Xiaowei Zhao, and Ye Han. An ensemble deep learning based predictor for simultaneously identifying protein ubiquitylation and sumoylation sites. *BMC Bioinformatics*, 22(1):519, October 2021.
 63. Hao Lv, Fu-Ying Dao, Zheng-Xing Guan, Hui Yang, Yan-Wen Li, and Hao Lin. Deep-kcr: accurate detection of lysine crotonylation sites using deep learning method. *Briefings in Bioinformatics*, 22(4):bbaa255, 10 2020.
 64. Hiroyuki Kurata, Md Harun-Or-Roshid, Sho Tsukiyama, and Kazuhiro Maeda. Predil13: Stacking a variety of machine and deep learning methods with esm-2 language model for identifying il13-inducing peptides. *Plos one*, 19(8):e0309078, 2024.
 65. Fan Zhang, Jinfeng Li, Zhenguang Wen, and Chun Fang. Fusb-esm2: Fusion model of protbert and esm-2 for cell-penetrating peptide prediction. *Computational Biology and Chemistry*, 111:108098, 2024.
 66. Yingheng Wang, Zichen Wang, Gil Sadeh, Luca Zancato, Alessandro Achille, George Karypis, and Huzefa Rangwala. Long-context protein language model. *bioRxiv*, pages 2024–10, 2024.
 67. Onat Dalmaz, Mahmut Yurt, and Tolga Çukur. Resvit: residual vision transformers for multimodal medical image synthesis. *IEEE Transactions on Medical Imaging*, 41(10):2598–2614, 2022.
 68. Fangyuan Kong, Mingxi Li, Songwei Liu, Ding Liu, Jingwen He, Yang Bai, Fangmin Chen, and Lean Fu. Residual local feature network for efficient super-resolution. In *Proceedings of the IEEE/CVF conference on computer vision and pattern recognition*, pages 766–776, 2022.
 69. Jesse Vig, Ali Madani, Lav R Varshney, Caiming Xiong, Richard Socher, and Nazneen Fatema Rajani. Bertology meets biology: Interpreting attention in protein language models. *arXiv preprint arXiv:2006.15222*, 2020.
 70. Davide Piras, Hiranya V Peiris, Andrew Pontzen, Luisa Lucie-Smith, Ningyuan Guo, and Brian Nord. A robust estimator of mutual information for deep learning interpretability. *Machine Learning: Science and Technology*, 4(2):025006, 2023.
 71. Mohamed Ishmael Belghazi, Aristide Baratin, Sai Rajeshwar, Sherjil Ozair, Yoshua Bengio, Aaron Courville, and Devon Hjelm. Mutual information neural estimation. In Jennifer Dy and Andreas Krause, editors, *Proceedings of the 35th International Conference on Machine Learning*, volume 80 of *Proceedings of Machine Learning Research*, pages 531–540. PMLR, 10–15 Jul 2018.
 72. Leland McInnes, John Healy, and James Melville. Umap: Uniform manifold approximation and projection for dimension reduction. *arXiv preprint arXiv:1802.03426*, 2018.
 73. Etienne Becht, Leland McInnes, John Healy, Charles-Antoine Dutertre, Immanuel WH Kwok, Lai Guan Ng, Florent Ginhoux, and Evan W Newell. Dimensionality reduction for visualizing single-cell data using umap.

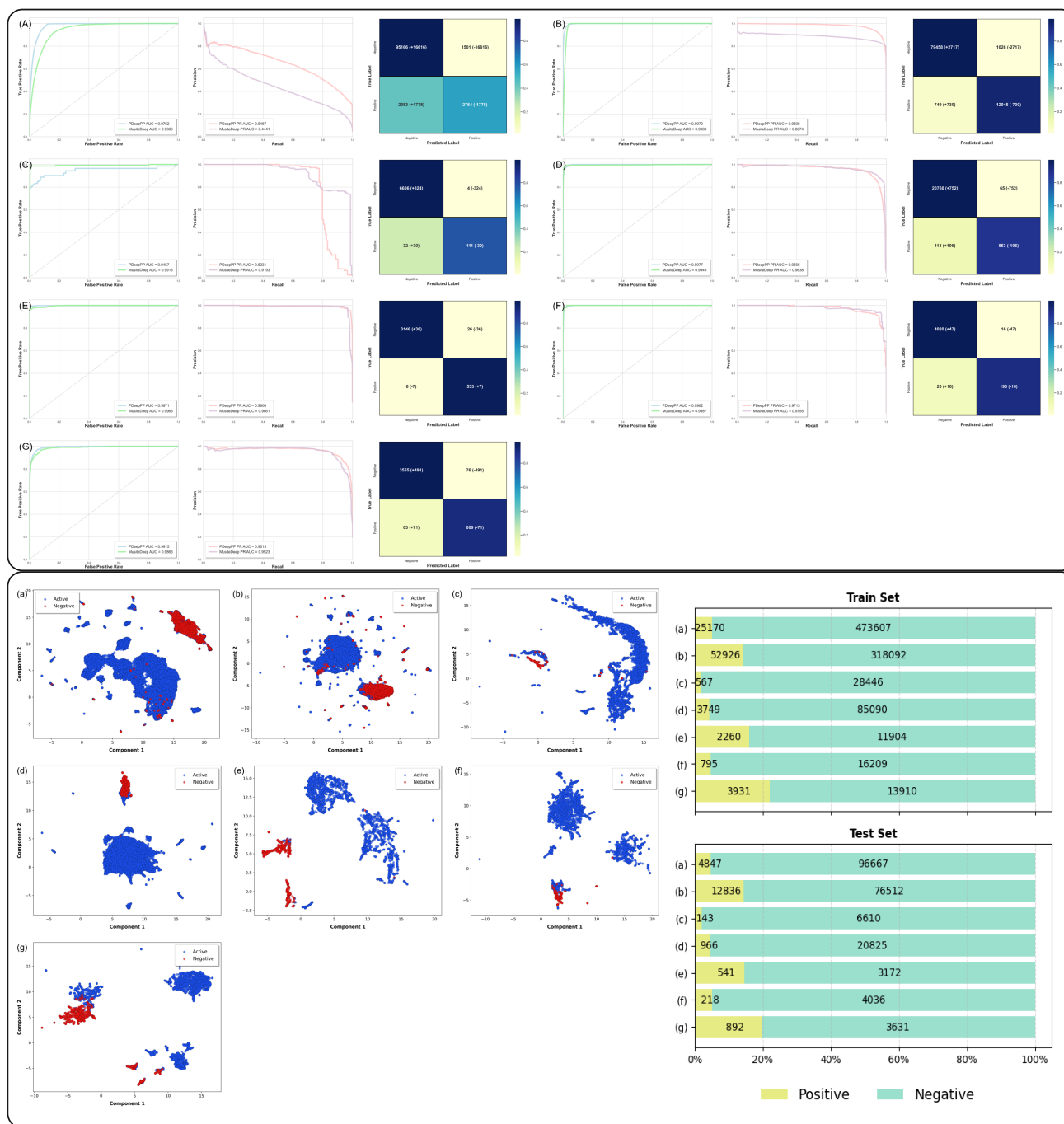
Nature biotechnology, 37(1):38–44, 2019.

74. Richard Meyes, Melanie Lu, Constantin Waubert de Puiseau, and Tobias Meisen. Ablation studies in artificial neural networks. *arXiv preprint arXiv:1901.08644*, 2019.

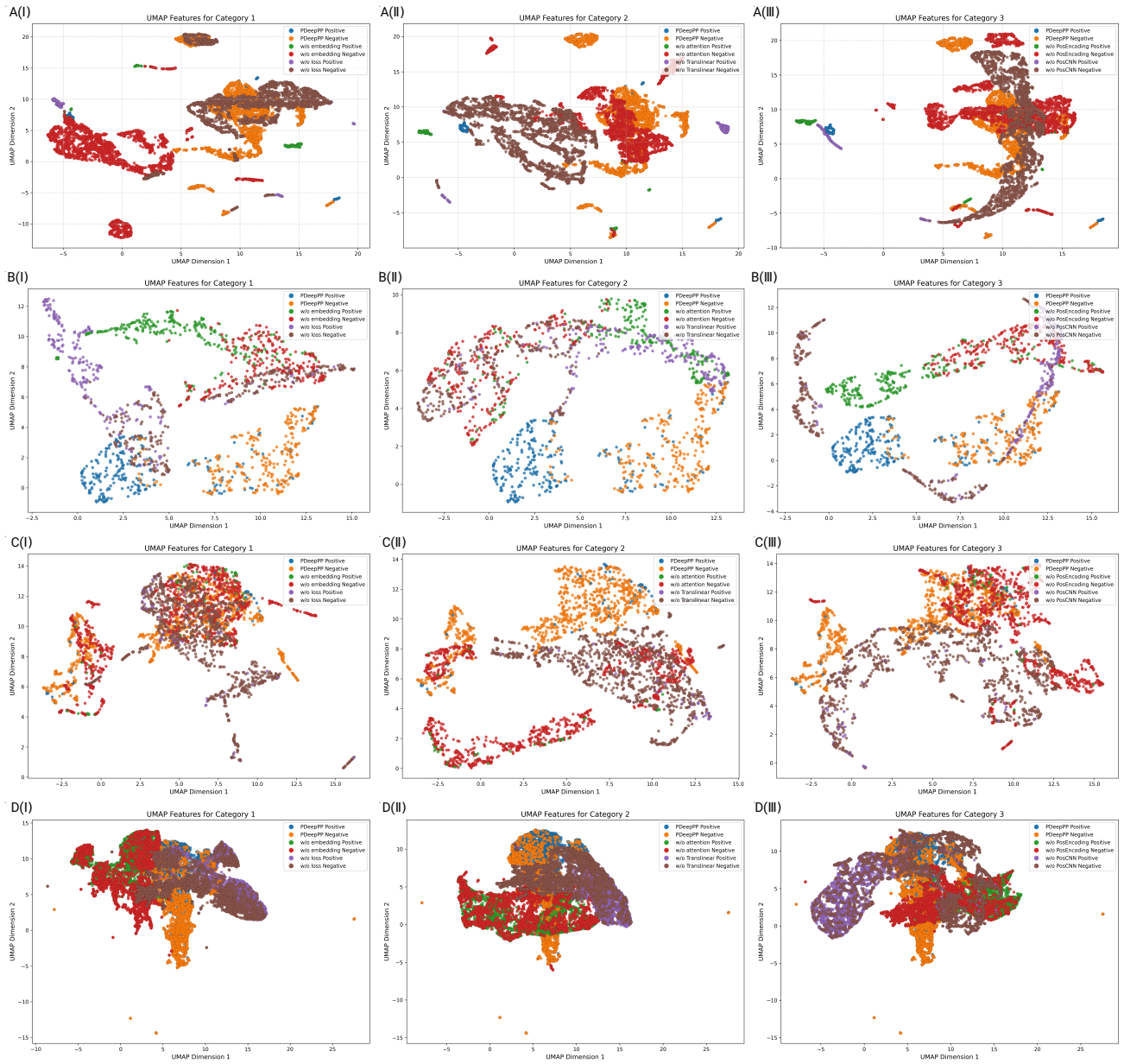
Supplementary



Supplementary Fig 1. The remaining ten tasks showing consistent performance in comparison with the UniDL4BioPep model. The upper section shows the AUC curves and confusion matrix combinations for each task. In the confusion matrices, the numbers in parentheses next to the values represent the difference in the count of this metric compared to PDeepPP for the UniDL4BioPep model. The color intensity of the matrix indicates the proportion of that class relative to the total negative/positive samples. The lower section displays the UMAP plots for each dataset after feature extraction by PDeepPP. The label order is: (A) ACE, (B) DPPIV, (C) bitter, (D) Quorum, (E) Anticancer_alternative, (F) Anti-MRSA, (G) Antiparasitic, (H) neuro, (I) Toxicity, (J) Antioxidant.



Supplementary Fig 2. The Remaining six tasks showing consistent performance in comparison with the MusiteDeep model. The upper section shows the AUC curves and confusion matrix combinations for each task. In the confusion matrices, the numbers in parentheses next to the values represent the difference in the count of that class relative to the total negative/positive samples. The color intensity of each block in the matrix indicates the proportion of that class relative to the total negative/positive samples. The lower section displays the UMAP plots for each dataset after feature extraction by PDeepPP, with the site distribution of these six datasets shown in the bottom right. The label order is: (A) Phosphoserine.Phosphothreonine.S,T, (B) N-linked-glycosylation_N, (C) O-linked-glycosylation.S,T, (D) Methylation_R, (E) S-Palmitoylation_C, (F) SUMOylation_K, (G) Hydroxyproline_P.



Supplementary Fig 3. Four datasets selected from existing datasets, with respect to the given category (see legend). UMAP plots are shown for each pair of related ablated models and the baseline model (PDeepPP) after feature extraction. (A)-(D) correspond to methylation-G, methylation-R, Ubiquitin-K*, and Crotonylation-K, respectively.

SuppTable 1. Benchmark Datasets Sourced from Publications Featuring State-of-the-Art Models

Tasks	Training dataset		Test dataset		Reference
	Positives	Negatives	Positives	Negatives	
Bioactivity					
ACE inhibitory activity	913	913	386	386	(41)
DPP IV inhibitory activity	532	532	133	133	(42)
Bitter	256	256	64	64	(43)
Umami	112	241	28	61	(44)
Antimicrobial activity	3876	9552	2584	6369	(45)
Antimalarial activity main	111	1708	28	427	(46)
alternaive	111	542	28	135	(46)
Quorum sensing activity	200	200	20	20	(47)
Anticancer activity main	689	689	172	172	(48; 49)
alternative	776	776	194	194	(48; 49)
Anti-MRSA strains activity	118	678	30	169	(50)
Tumor T cell antigens	470	318	122	75	(51)
Blood–Brain Barrier	100	100	19	19	(52)
Antiparasitic activity	255	255	46	46	(53)
Neuropeptide	1940	1940	485	485	(54; 55)
Antibacterial activity	6583	6583	1695	1695	(56)
Antifungal activity	778	778	215	215	(56)
Antiviral activity	2321	2321	623	623	(56)
Toxicity	1642	1642	290	290	(57)
Antioxidant activity	582	541	146	135	(58)
PTMs(23)					
Phosphoserine/threonine	25170	473607	4847	96667	
Phosphotyrosine	6939	64884	1669	17123	
N-linked glycosylation	52926	318092	12836	76512	
O-linked glycosylation	567	28446	143	6610	
N6-acetyllysine	16222	199649	3895	48653	
Methylarginine	3749	85090	966	20825	
Methyllysine	1324	25836	335	7640	
S-palmitoylation-cysteine	2260	11904	541	3172	
Pyridoxine-carboxylic-acid	1128	7688	285	1554	
Ubiquitination	2528	26772	581	7797	
SUMOylation	795	16209	218	4036	
Hydroxylysine	390	2968	121	661	
Hydroxyproline	3931	13910	892	3631	
Remaining PTMs					
methylation-G	627	10490	165	2615	(60)
methylation-R	1038	1038	290	290	(61)
Ubiquitin_K*	2528	26772	581	7797	(62)
Crotonylation_K	6975	6975	3989	3989	(63)

SuppTable 2. Comparison with UniDL4BioPep in bioactive peptides and state-of-the-art models from the same benchmark datasets

Bioactivity	Model name	ACC	ROC	PR	BACC	Sn	Sp	MCC
ACE inhibitory activity	PDeepPP	0.8225	0.9049	0.9144	0.8225	0.8782	0.7668	0.6491
	UniDL4BioPep	0.8433	0.8918	0.8728	0.8433	0.8238	0.8627	0.6870
	mAHTPred	0.883	0.951		N/A	0.894	0.873	0.767
DPP IV inhibitory activity	PDeepPP	0.8947	0.9615	0.9654	0.8947	0.8496	0.9398	0.7927
	UniDL4BioPep	0.8534	0.9384	0.9444	0.8534	0.8647	0.8421	0.7069
	iDPPIV-SCM	0.797	0.847		N/A	0.789	0.805	0.594
Bitter	PDeepPP	0.9141	0.9625	0.9692	0.9141	0.8906	0.9375	0.8290
	UniDL4BioPep	0.9375	0.9824	0.9838	0.9375	0.9219	0.9531	0.8754
	BERT4Bitter	N/A	0.922		0.938	0.906	0.844	0.964
	iBitter-Fuse	0.93	0.933		N/A	0.938	0.922	0.859
Umami	PDeepPP	0.9213	0.9543	0.9835	0.9330	0.9016	0.9643	0.8325
	UniDL4BioPep	0.8764	0.9417	0.9760	0.8326	0.9508	0.7143	0.7055
	UniDL4BioPep-FL	0.888	0.943		0.883	0.892	0.875	0.733
	iUmami-SCM	0.865	0.898		N/A	0.714	0.934	0.679
Antimicrobial activity	PDeepPP	0.9726	0.9947	0.9977	0.9609	0.9887	0.9330	0.9329
	UniDL4BioPep	0.9631	0.9910	0.9959	0.9532	0.9768	0.9296	0.9099
	UniDL4BioPep-FL	0.96	0.991		0.961	0.96	0.963	0.903
	TransImbAMP	N/A	N/A		0.969	0.963	0.974	N/A
Antimalarial activity (main dataset)	PDeepPP	0.9758	0.9049	0.9898	0.8203	0.9977	0.6429	0.7695
	UniDL4BioPep	0.9780	0.8898	0.9872	0.8214	1.0000	0.6429	0.7926
	UniDL4BioPep-FL	0.978	0.898		0.965	0.979	0.95	0.793
	iAMAP-SCM	0.978	0.82		0.826	0.654	0.998	0.776
Antimalarial activity (alternative dataset)	PDeepPP	0.9877	0.9929	0.9984	0.9643	1.0000	0.9286	0.9566
	UniDL4BioPep	0.9816	0.9844	0.9965	0.9464	1.0000	0.8929	0.9346
	UniDL4BioPep-FL	0.989	0.987		0.993	0.985	1	0.9570
	iAMAP-SCM	0.957	0.903		0.896	0.808	0.985	0.834
Quorum sensing activity	PDeepPP	0.9750	0.9975	0.9976	0.9750	0.9500	1.0000	0.9512
	UniDL4BioPep	0.9500	0.9900	0.9908	0.9500	0.9000	1.0000	0.9045
	iQSP	0.93	0.96		N/A	N/A	N/A	0.86
	QSPred-FL	0.943	0.945		N/A	0.935	0.95	0.885
Anticancer activity (main dataset)	PDeepPP	0.7587	0.8334	0.8308	0.7587	0.8547	0.6628	0.5272
	UniDL4BioPep	0.7355	0.8054	0.7780	0.7355	0.7326	0.7384	0.4709
	iACP-FSCM	0.825	0.812		0.825	0.726	0.903	0.646
	AntiCP2.0	0.754	N/A		0.754	0.774	0.734	0.51
Anticancer activity (alternative dataset)	PDeepPP	0.9433	0.9709	0.9668	0.9433	0.9639	0.9227	0.8874
	UniDL4BioPep	0.9459	0.9711	0.9630	0.9459	0.9794	0.9124	0.8938
	iACP-FSCM	0.889	0.93		N/A	0.876	0.902	0.779
	AntiCP2.0	0.92	N/A		N/A	0.923	0.918	0.84
Anti-MRSA strains activity	PDeepPP	0.9950	0.9998	1.0000	0.9833	1.0000	0.9667	0.9803
	UniDL4BioPep	0.9899	0.9986	0.9998	0.9667	1.0000	0.9333	0.9604
	UniDL4BioPep-FL	0.994	0.999		0.997	0.994	1	0.98
	SCMRSA	0.96	0.986		0.935	0.9	0.97	0.848
Tumor T cell antigens	PDeepPP	0.7563	0.8198	0.7662	0.7185	0.5600	0.8770	0.4680
	UniDL4BioPep	0.7513	0.7883	0.7395	0.7144	0.5600	0.8689	0.4569
	UniDL4BioPep-FL	0.746	0.796		0.762	0.734	0.791	0.446
	iTTCA-Hybrid	0.71	0.756		N/A	0.844	0.493	0.363
Blood-Brain Barrier	PDeepPP	0.9211	0.9640	0.9680	0.9211	0.9474	0.8947	0.8433
	UniDL4BioPep	0.8421	0.9224	0.9211	0.8421	0.8947	0.7895	0.6880
	BBPred	0.7895	0.7895		N/A	0.6316	0.9474	0.6102
Antiparasitic activity	PDeepPP	0.7609	0.9267	0.9370	0.7609	0.9565	0.5652	0.5669
	UniDL4BioPep	0.8478	0.9045	0.9258	0.8478	0.8043	0.8913	0.6983
	PredAPP	0.88	0.922		N/A	0.978	0.783	0.775
Neuropeptide	PDeepPP	0.9021	0.9611	0.9602	0.9021	0.9010	0.9031	0.8041
	UniDL4BioPep	0.9052	0.9707	0.9707	0.9052	0.8784	0.9320	0.8115
	PreNeuroP	0.897	0.954		N/A	0.886	0.907	0.794
	NeuroPred-CLQ	0.936	0.988		N/A	0.897	0.975	0.875
Antibacterial activity	PDeepPP	0.9478	0.9811	0.9752	0.9478	0.9617	0.9339	0.8959
	UniDL4BioPep	0.9395	0.9775	0.9704	0.9395	0.9687	0.9103	0.8806
	ABPDiscover	0.935	0.975		N/A	0.912	0.957	0.87
Antifungal activity	PDeepPP	0.9535	0.9911	0.9916	0.9535	0.9442	0.9628	0.9071
	UniDL4BioPep	0.9512	0.9862	0.9838	0.9512	0.9628	0.9395	0.9026
	ABPDiscover	0.942	0.988		N/A	0.921	0.963	0.884
Antiviral activity	PDeepPP	0.8531	0.9192	0.9164	0.8531	0.9486	0.7576	0.7195
	UniDL4BioPep	0.8291	0.9012	0.8827	0.8291	0.9037	0.7544	0.6656
	ABPDiscover	0.828	0.896		N/A	0.764	0.892	0.662
Toxicity	PDeepPP	0.9172	0.9779	0.9770	0.9168	0.9108	0.9228	0.8336
	UniDL4BioPep	0.9603	0.9943	0.9934	0.9608	0.9665	0.9550	0.9205
	ATSE	0.952	0.976		N/A	0.965	0.94	0.903
Antioxidant activity	PDeepPP	0.7972	0.8776	0.8880	0.7981	0.7740	0.8222	0.5959
	UniDL4BioPep	0.8221	0.9296	0.9410	0.8229	0.8014	0.8444	0.6454
	AntiOxPred-FRS	N/A	0.79		N/A	N/A	N/A	0.48

SuppTable 3. Comparison with the MusiteDeep in PTMs from the same benchmark datasets

PTM types	Model	ACC	ROC	PR	BACC	SN	SP	MCC
Hydroxyproline	PDeepPP	0.9885	0.9992	0.9959	0.9729	0.9504	0.9955	0.9557
	MusiteDeep	0.9425	0.9937	0.9718	0.9626	0.9917	0.9334	0.8219
Hydroxylysine	PDeepPP	0.9648	0.9915	0.9615	0.9430	0.9070	0.9791	0.8887
	MusiteDeep	0.8720	0.9866	0.9523	0.9152	0.9865	0.8438	0.7084
Methyllysine	PDeepPP	0.9984	0.9997	0.9972	0.9924	0.9859	0.9990	0.9809
	MusiteDeep	0.9877	0.9921	0.9649	0.9842	0.9803	0.9881	0.8756
Methylarginine	PDeepPP	0.9918	0.9977	0.9565	0.9400	0.8830	0.9969	0.9016
	MusiteDeep	0.9622	0.9949	0.9638	0.9768	0.9928	0.9608	0.7173
N-linked glycosylation	PDeepPP	0.9810	0.9970	0.9806	0.9644	0.9415	0.9873	0.9204
	MusiteDeep	0.9597	0.9883	0.8874	0.9760	0.9985	0.9535	0.8579
N6-acetyllysine	PDeepPP	0.9870	0.9959	0.9589	0.9491	0.9045	0.9936	0.9049
	MusiteDeep	0.9647	0.9939	0.9105	0.9761	0.9895	0.9627	0.8042
Phosphotyrosine	PDeepPP	0.9944	0.9989	0.9909	0.9818	0.9664	0.9971	0.9654
	MusiteDeep	0.9568	0.9943	0.9417	0.9709	0.9880	0.9538	0.7971
Phosphoserine/threonine	PDeepPP	0.9984	0.9872	0.9910	0.9819	0.9738	0.9899	0.9546
	MusiteDeep	0.9977	0.9837	0.9871	0.9740	0.9596	0.9885	0.9416
Pyrrolidone-carboxylic-acid	PDeepPP	0.9804	0.9964	0.9822	0.9626	0.9368	0.9884	0.9253
	MusiteDeep	0.9625	0.9978	0.9910	0.9735	0.9895	0.9575	0.8749
O-linked glycosylation	PDeepPP	0.9941	0.9050	0.8193	0.8738	0.7483	0.9994	0.8466
	MusiteDeep	0.9511	0.9916	0.9193	0.9682	0.9860	0.9504	0.5303
S-palmitoylation-cysteine	PDeepPP	0.9908	0.9971	0.9906	0.9885	0.9852	0.9918	0.9639
	MusiteDeep	0.9793	0.9965	0.9861	0.9764	0.9723	0.9805	0.9207
SUMOylation	PDeepPP	0.9915	0.9982	0.9713	0.9521	0.9083	0.9960	0.9123
	MusiteDeep	0.9843	0.9987	0.9755	0.9830	0.9817	0.9844	0.8633
Ubiquitination	PDeepPP	0.9922	0.9983	0.9794	0.9656	0.9346	0.9965	0.9394
	MusiteDeep	0.9390	0.9819	0.8969	0.9457	0.9535	0.9379	0.6874

SuppTable 4. Model Hyperparameter Configuration

Category	Parameter	Value	Description
Training Config	Learning Rate	0.001	Initial learning rate for Adam optimizer
	Batch Size	32/128	Training batch size (32) and inference batch size (128)
	Training Epochs	100	Maximum training iterations with early stopping
	Patience	20	Epochs tolerance for validation loss plateau
Architecture	ESM-2 Dimension	1280	Output dimension of pretrained ESM-2 embeddings
	Transformer Dim	128	Hidden dimension in self-attention layers
	Attention Heads	8	Parallel attention mechanisms per layer
	Encoder Layers	4	Stacked transformer encoder blocks
	CNN Channels	64→32→64	Feature channel progression in convolutional modules
Regularization	Dropout	0.3/0.15	Dropout rates: attention (0.3), CNN (0.15)
	Position Encoding	Yes	Learnable positional embeddings
	Weight Decay	None	No explicit L2 regularization applied
UMAP Visualization	n_neighbors	15	Local neighborhood size for manifold approximation
	min_dist	0.1	Minimum embedding distance between points
	random_state	42	Seed for reproducible visualization
Loss Function	λ	[0.9,1.0]	Cross-entropy weight in TIM loss
	α	1.0	Entropy regularization coefficient
	Threshold	0.5	Decision boundary for classification
Feature Fusion	ESM Ratio	[0.9,1.0]	Weighting between ESM-2 and task-specific embeddings

Notes:

1. Final testing uses optimal parameters
2. UMAP parameters specifically used for 2D projection of 1280D feature vectors in model interpretability analysis. The n_neighbors controls local/global structure balance, min_dist affects cluster tightness, and random_state ensures reproducibility.
3. Implementation: Based on PyTorch 1.12+ framework